

Article

A Responsible Machine Learning Workflow

With Focus on Interpretable Models, Post-hoc Explanation, and Discrimination Testing

Navdeep Gill ^{1,†}, Patrick Hall ^{1,3,†,*}, Kim Montgomery ^{1,†}, and Nicholas Schmidt ^{2,†}

¹ H2O.ai

² BLDS, LLC

³ George Washington University

* Correspondence: phall@h2o.ai; nschmidt@bldslc.com

† All authors contributed equally to this work.

Version January 29, 2020 submitted to Information

Abstract: This manuscript outlines a viable approach for training and evaluating machine learning (ML) systems for high-stakes, human-centered, or regulated applications using common Python programming tools. The accuracy and intrinsic interpretability of two types of constrained models, monotonic gradient boosting machines (MGBM) and explainable neural networks (XNN), a deep learning architecture well-suited for structured data, are assessed on simulated data and publicly available mortgage data. For maximum transparency and the potential generation of personalized adverse action notices, the constrained models are analyzed using post-hoc explanation techniques including plots of partial dependence (PD) and individual conditional expectation (ICE) and global and local Shapley feature importance. The constrained model predictions are also tested for disparate impact (DI) and other types of discrimination using measures with long-standing legal precedents, adverse impact ratio (AIR), marginal effect (ME), standardized mean difference (SMD), and also with straightforward group fairness measures. By combining interpretable models, post-hoc explanation, and discrimination testing with accessible software tools, this text aims to provide a template workflow for important ML applications that require high accuracy and interpretability and that mitigate risks of discrimination.

Keywords: Machine Learning; Neural Network; Gradient Boosting Machine; Interpretable; Explanation; Fairness; Disparate Impact; Python

0. Introduction

Responsible artificial intelligence (AI) has been variously conceptualized as AI-based products or projects that use transparent technical mechanisms, that create appealable decisions or outcomes, that perform reliably and in a trustworthy manner over time, that exhibit minimal social discrimination, and that are designed by humans with diverse experiences, both in terms of demographics and professional backgrounds.¹ Although responsible AI is today a somewhat broad and amorphous notion, at least one aspect is becoming clear. ML models, a common application of AI, can present serious risks. ML models can be inaccurate and unappealable black-boxes, even with the application of newer post-hoc explanation techniques [1].² ML models can perpetuate and exacerbate discrimination [2], [3], [4]. ML models can be hacked, resulting in manipulated model outcomes or the exposure

¹ See: [Responsible Artificial Intelligence](#), [Responsible AI: A Framework for Building Trust in Your AI Solutions](#), PwC's Responsible AI, Responsible AI Practices.

² See: [When a Computer Program Keeps You in Jail](#).

of proprietary intellectual property or sensitive training data [5], [6], [7], [8]. This manuscript makes no claim that these interdependent issues of opaqueness, discrimination, privacy harms, and security vulnerabilities in ML have been resolved, even as singular entities, and much less as complex intersectional phenomena. However, Sections 1, 2, and 3 do propose some specific technical countermeasures, in the form interpretable models, post-hoc explanation, and DI and discrimination testing implemented in widely available Python tools, that responsible practitioners can use to address a subset of these vexing problems.^{3,4}

Section 1 describes methods and materials, including collected training datasets, interpretable and constrained models, post-hoc explanations, tests for DI and other social discrimination, and public and open source software resources associated with this text. In Section 2, interpretable and constrained modeling results are compared to less interpretable and unconstrained models, and post-hoc explanation and discrimination testing results are also presented for interpretable models. Of course, an even wider array of tools and techniques are likely helpful to fully minimize discrimination, inaccuracy, privacy, and security risks associated with ML models. Section 3 puts forward a more holistic responsible ML modeling workflow, and addresses the burgeoning Python ecosystem for responsible AI, along with appeal and override of automated decisions, and discrimination testing and remediation in practice. Section 4 closes this manuscript with a brief summary of the outlined methods, materials, results, and discussion.

1. Materials and Methods

The simulated data (see Subsection 1.1) is based on the well-known Friedman datasets. Its known feature importance and discrimination characteristics are used to gauge the validity of interpretable modeling, post-hoc explanation, and discrimination testing techniques [10], [11]. The mortgage data (see Subsection 1.2) is sourced from the Home Mortgage Disclosure Act (HMDA) database and is a fairly realistic data source for demonstrating the template workflow.⁵ To provide a sense of accuracy differences, performance of more interpretable constrained ML models and less interpretable unconstrained ML models is compared on simulated data and collected mortgage data. Because the unconstrained ML models, gradient boosting machines (GBMs) (e.g. [12], [13]) and artificial neural networks (ANNs) (e.g. [14], [15], [16], [17]), do not exhibit convincing accuracy benefits on the simulated or mortgage data and can also present previously delineated risks, further explanation and discrimination analysis are applied only to the constrained, interpretable ML models [1], [18], [19]. Here, MGBMs⁶ (See subsection 1.3) and XNNs (see Subsection 1.4, [20] [21]) will serve as those more interpretable models for subsequent explanatory and discrimination analyses. MGBM and XNN interpretable model architectures are selected for this text because they are straightforward variants of popular unconstrained ML models. If practitioners are working with GBM and ANN models, it should be relatively uncomplicated to also evaluate the constrained versions of these models.

The same can be said of the selected explanation methods and discrimination tests. Due to their post-hoc nature, they can often be shoe-horned into existing ML workflows and pipelines. Presented explanation techniques include PD and ICE (see Subsection 1.5) and Shapley values (see Subsection 1.6) [13], [22], [23], [24]. PD, ICE, and Shapley values provide direct, global, and local summaries and descriptions of constrained models without resorting to the use of intermediary and approximate

³ This text and associated software are not, and should not be construed as, legal advice or requirements for regulatory compliance.

⁴ In the United States (US), interpretable models, explanations, DI testing, and the model documentation they enable may be required under the Civil Rights Acts of 1964 and 1991, the Americans with Disabilities Act, the Genetic Information Nondiscrimination Act, the Health Insurance Portability and Accountability Act, the Equal Credit Opportunity Act (ECOA), the Fair Credit Reporting Act (FCRA), the Fair Housing Act, Federal Reserve SR 11-7, and the European Union (EU) Greater Data Privacy Regulation (GDPR) Article 22 [9].

⁵ See: [Mortgage data \(HMDA\)](#).

⁶ As implemented in [XGBoost](#) or [h2o](#).

surrogate models. Discussed discrimination testing methods (see Subsection 1.7) include AIR, ME, SMD, and confusion matrix metrics [2], [25], [26].⁷ Accuracy and other confusion matrix metrics are also reported by demographic segment [27]. All outlined materials and methods are implemented in open source Python code, and are made available through GitHub (see Subsection 1.8).

1.1. Simulated Data

Simulated data is created based on a function first proposed in Friedman [10] and extended in Friedman *et al.* [11]:

$$f(\mathbf{X}) = 10 \sin(\pi \mathbf{X}_{\text{Friedman},1} \mathbf{X}_{\text{Friedman},2}) + 20(\mathbf{X}_{\text{Friedman},3} - 0.5)^2 + 10 \mathbf{X}_{\text{Friedman},4} + 5 \mathbf{X}_{\text{Friedman},5} \quad (1)$$

where $\mathbf{X}_{\text{Friedman},j}$ are random uniform features in $[0, 1]$. In Friedman's texts, a Gaussian noise term was added to create a continuous output feature for testing spline regression methodologies. In this manuscript, the signal generating function and input features are modified in several ways. Two binary features, a categorical feature with five discrete levels, and a bias term are introduced into f to add a degree of complexity that may more closely mimic real-world settings. For binary classification analysis, the Gaussian noise term is replaced with noise drawn from a logistic distribution and coefficients are re-scaled to be one fifth of the size of those used by Friedman, and any $f(\mathbf{X})$ value above 0 is classified as a positive outcome, while $f(\mathbf{X})$ values less than or equal to zero are designated as negative outcomes. Finally, f is augmented with two hypothetical protected class-control features with known dependencies on the binary outcome to allow for discrimination testing. The simulated data is generated to have eight input features, twelve after numeric encoding of categorical features, and a binary outcome, two class-control features, and 100,000 rows. The simulated data is then split into a training and test set, with 80,000 and 20,000 observations, respectively. Within the training set, a 5 fold cross validation indicator is used for training all models. For an exact specification of the simulated data, see the software resources referenced in Subsection 1.8.

1.2. Mortgage Data

The mortgage dataset analyzed here is a random sample of consumer-anonymized loans from the HMDA database. These loans are a subset of all originated mortgage loans in the 2018 HMDA data that were chosen to represent a relatively comparable group of consumer mortgages. A selection of features is used to predict whether a loan is *high-priced*, i.e., the annual percentage rate (APR) charged was 150 basis points (1.5%) or more above a survey-based estimate of other similar loans offered around the time of the given loan. After data cleaning and preprocessing to encode categorical features and create missing markers, the mortgage data contains ten input features and the binary outcome, *high-priced*. The data is split into a training set with 160,338 loans and a marker for 5 fold cross validation and a test set containing 39,662 loans. While lenders would almost certainly use more information than the selected features to determine whether to offer and originate a high-priced loan, the selected input features (LTV ratio, DTI ratio, property value, loan amount, introductory interest rate, customer income, etc.) are likely to be some of the most influential factors that a lender would consider. See Appendix A for general information regarding HMDA data.

1.3. Monotonic Gradient Boosting Machine

MGBMs constrain typical GBM training to consider only tree splits that obey user-defined positive and negative monotonicity constraints, with respect to each X_j and y independently. The MGBM

⁷ Part 1607 - Uniform Guidelines on Employee Selection Procedures (1978) §1607.4.

remains an additive combination of B trees trained by gradient boosting, T_b , and each tree learns a set of splitting rules that respect monotonicity constraints, Θ_b^{mono} .

$$g^{\text{MGBM}}(\mathbf{x}) = \sum_{b=1}^B T_b(\mathbf{x}; \Theta_b^{\text{mono}}) \quad (2)$$

As in unconstrained GBM, Θ_b^{mono} is selected in a greedy, additive fashion by minimizing a regularized loss function that considers known target labels, \mathbf{y} , the predictions of all subsequently trained trees in the in g^{MGBM} , $g_{b-1}^{\text{MGBM}}(\mathbf{X})$, and the b -th tree splits, $T_b(\mathbf{x}^{(i)}; \Theta_b^{\text{mono}})$, in a numeric error function (e.g., squared error, Huber error), l , and a regularization term that penalizes complexity in the current tree, $\Omega(T_b)$.

Herein, two g^{MGBM} models are trained. One on the simulated data and one on the mortgage data. In both cases, positive and negative monotonic constraints for each X_j are selected using domain knowledge, random grid search is used to determine other hyperparameters, and five-fold cross validation and test partitions are used for model assessment. See Appendices B.1 and B.2 for details pertaining to MGBM training. For exact parameterization of the two g^{MGBM} models, see the software resources referenced in Subsection 1.8.

1.4. Explainable Neural Network

XNNs are an alternative formulation of additive index models in which the ridge functions are neural networks [20]. XNNs also bear a strong resemblance to generalized additive models (GAMs) and so-called explainable boosting machines (EBMs or GA²M), i.e., GAMs which consider main effects and a small number of 2-way interactions and may also incorporate boosting into their training [13], [28]. Hence, XNNs enable users to tailor interpretable neural network architectures to a given prediction problem and to visualize model behavior by plotting ridge functions. XNNs are composed of a global bias term, μ_0 , K individually specified neural networks, n_k with scale parameters γ_k , and the inputs to each n_k are themselves a linear combination of modeling inputs, $\sum_j \beta_{k,j} x_j$.

$$g^{\text{XNN}}(\mathbf{x}) = \mu_0 + \sum_{k=0}^{K-1} \gamma_k n_k \left(\sum_{j=0}^{J=P-1} \beta_{k,j} x_j \right) \quad (3)$$

Here, each g^{XNN} is trained by mini-batch stochastic gradient descent (SGD) on the simulated data and mortgage data. Each g^{XNN} is assessed in five training folds and in a test data partition. L_1 regularization is applied to both the projection and combination layers to induce a sparse and interpretable model, where each n_k subnetwork and corresponding combination layer γ_k are ideally associated with an important X_j or combination thereof. The g^{XNN} models appear highly sensitive to weight initialization and batch size. Be aware that g^{XNN} model architectures may require manual and judicious feature selection due to long training times. For more details regarding g^{XNN} training, see the software resources in Subsection 1.8 and Appendices B.1 and B.3.

1.5. One-dimensional Partial Dependence and Individual Conditional Expectation

PD plots are a widely-used method for describing and plotting the average predictions of a complex model g across some partition of data \mathbf{X} for some interesting input feature X_j [13]. ICE plots are a newer method that describes the local behavior of g for a single instance $\mathbf{x} \in \mathcal{X}$ [22]. PD and ICE can be overlaid in the same plot to compensate for known weaknesses of PD (e.g., inaccuracy in the presence of strong interactions and correlations [22], [29]), to identify interactions modeled by g , and to create a holistic global and local portrait of the predictions for some g and X_j [22]. For details regarding the calculation of one-dimensional PD and ICE, see the software resources in Subsection 1.8 and Appendices B.1 and B.4.

1.6. Shapley Values

Shapley explanations are a class of additive, locally accurate feature contribution measures with long-standing theoretical support [23], [30]. Shapley explanations are the only possible locally accurate and globally consistent feature contribution values, meaning that Shapley explanation values for input features always sum to $g(\mathbf{x})$ for some $\mathbf{x} \in \mathcal{X}$ and that Shapley explanation values should never decrease in magnitude for some x_j when g is changed such that x_j truly makes a stronger contribution to $g(\mathbf{x})$ [23], [24].

Shapley values can be estimated in different ways, many of which are intractable for datasets with large \mathcal{P} . Tree SHAP is a specific implementation of Shapley explanations that relies on traversing internal decision tree structures to efficiently estimate the contribution of each x_j for some $g(\mathbf{x})$ [24]. Tree SHAP (SHapley Additive exPlanations) has been implemented efficiently in popular gradient boosting libraries such as `h2o`, `LightGBM`, and `XGBoost`, and Tree SHAP is used to calculate accurate and consistent global and local feature importance for MGBM models in Sections 1 and 2. Deep SHAP is an approximate Shapley value technique that creates SHAP values for ANNs [23]. Deep SHAP is implemented in the `shap` package and is used to generate SHAP values for the two g^{XNN} models discussed in Sections 1 and 2. For more information pertaining to the calculation of Shapley values, see Appendices B.1 and B.5.

1.7. Discrimination Testing Metrics

Because many technical and academic discussions of fairness in ML have been inconclusive⁸, this text will draw on regulatory and legal standards that have been used for years in industries like Financial Services. The discussed metrics are also representative of fair lending analyses and pair well with the mortgage data. See Appendix C for a brief discussion regarding different types of discrimination under US laws and Appendix D for remarks on statistical vs. practical significance for discrimination measure values.

One measure is known as marginal effects (ME). ME is simply the difference between the percent of the control group members receiving a favorable outcome and the percent of the protected class members receiving a favorable outcome.

$$ME \equiv 100 \cdot (\Pr(\hat{\mathbf{y}} = 1 | X_c = 1) - \Pr(\hat{\mathbf{y}} = 1 | X_p = 1)) \quad (4)$$

where X_p and X_c represent binary markers created from some demographic attribute, c denotes the control group (often whites or males), and p indicates a protected group. ME is a favored DI metric used by the CFPB, the primary agency charged with regulating fair lending laws at the largest US lending institutions and various other participants in the consumer financial market.⁹ Another important measure of DI is adverse impact ratio (AIR), more commonly known as a *relative risk ratio* in settings outside of regulatory compliance.

$$AIR \equiv \frac{\Pr(\hat{\mathbf{y}} = 1 | X_p = 1)}{\Pr(\hat{\mathbf{y}} = 1 | X_c = 1)} \quad (5)$$

AIR is equal to the ratio of the proportion of the protected class that receives a favorable outcome divided by the proportion of the control class that receives a favorable outcome. Another long-standing measure of DI is standardized mean difference (SMD). SMD is often used to assess disparities in continuous features, such as income differences in employment analyses, or interest rate differences in lending. It originated from work on statistical power, and is more formally known as *Cohen's d*. SMD is equal to the difference in the average class outcomes minus the control class outcome, divided by a

⁸ See: [Tutorial: 21 Fairness Definitions and Their Politics](#).

⁹ See: [Supervisory Highlights, Issue 9, Fall 2015](#).

measure of the standard deviation of the population.¹⁰ Cohen defined values of this metric to have *small*, *medium*, and *large* effect sizes if the values exceeded 0.2, 0.5, and 0.8, respectively.

$$\text{SMD} \equiv \frac{\bar{\hat{y}}_p - \bar{\hat{y}}_c}{\sigma_{\hat{y}}} \quad (6)$$

The numerator in the SMD is equivalent to marginal effects but adds the standard deviation divisor as a standardizing factor. Because of this standardization factor, SMD allows for a comparison across different types of outcomes, such as inequity in mortgage closing fees or inequities in the interest rates given on certain loans. In this, one may apply definitions in Cohen [25] of *small*, *medium*, and *large* effect sizes, which represent a measure of *practical significance*, which is described in detail below. Finally, confusion matrix metrics and their ratios in demographic groups are also considered as measures of DI in section 2.

1.8. Software Resources

Python code to reproduce discussed results is available at: <https://github.com/h2oai/article-information-2019>. The primary Python packages employed are: `numpy` and `pandas` for data manipulation, `h2o`, `keras`, `shap`, and `tensorflow` for modeling, explanation, and discrimination testing, and `matplotlib` for plotting.

2. Results

Results are laid out for the simulated and mortgage datasets. Accuracy is compared for unconstrained, less interpretable g^{GBM} and g^{ANN} models and constrained, more interpretable g^{MGBM} and g^{XNN} models. Then, for the g^{MGBM} and g^{XNN} models, intrinsic interpretability, post-hoc explanation, and discrimination testing results are presented.

2.1. Mortgage Data Results

Results for the mortgage data are presented in Subsections 2.1.1 – 2.1.3. g^{ANN} and g^{XNN} outperform g^{GBM} and g^{MGBM} on the mortgage data, but as in Subsection E.1 the constrained variants of both model architectures do not show large differences in model performance with respect to unconstrained variants. Assuming that small fit differences on static test data do not outweigh the need for intrinsic model interpretability and reliable post-hoc explainability in high-stakes, human-centered, or regulated applications, only g^{MGBM} and g^{XNN} interpretability, post-hoc explainability, and discrimination testing results are presented.

2.1.1. Constrained vs. Unconstrained Model Fit Assessment

Table 1 shows that g^{ANN} and g^{XNN} noticeably outperform g^{GBM} and g^{MGBM} on the mortgage data. This is at least partially due to the preprocessing required to present directly comparable post-hoc explainability results and to use neural networks and tensorflow, e.g., numerical encoding of categorical features and missing values. This preprocessing appears to hamstring some of the tree-based models' inherent capabilities. g^{GBM} models trained on non-encoded data with missing values repeatedly produced AUC values of ~ 0.81 (not shown, but available in resources discussed in Subsection 1.8).

¹⁰ There are several measures of the standard deviation of the score that are typically used: 1. the standard deviation of the population, irrespective of protected class status, 2. a standard deviation calculated only over the two groups being considered in a particular calculation, or 3. a pooled standard deviation, using the standard deviations for each of the two groups with weights.

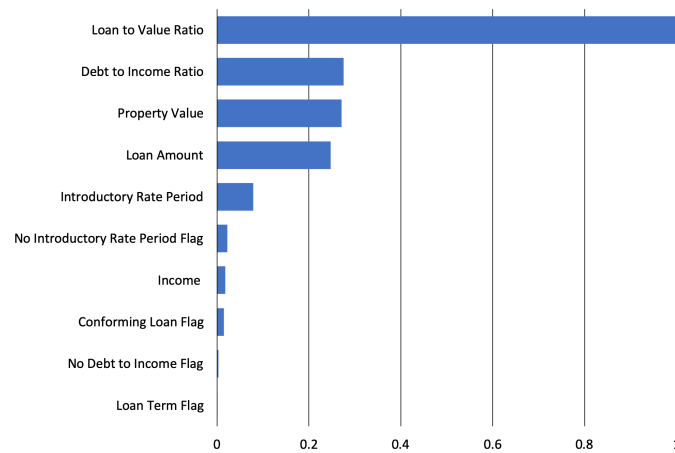
Table 1. Fit metrics for g^{GBM} , g^{MGBM} , g^{ANN} , and g^{XNN} on the mortgage test data.

Model	Accuracy	AUC	Logloss	RMSE
g^{GBM}	0.795	0.828	0.252	0.276
g^{MGBM}	0.765	0.814	0.259	0.278
g^{ANN}	0.865	0.871	0.231	0.262
g^{XNN}	0.869	0.868	0.233	0.263

Regardless of the fit differences between the two families of hypothesis models, the difference between the fit of constrained and unconstrained variants within the two types of models is small for the GBMs and negligible for ANNs, 3% and < 1% worse fit respectively, averaged across the metrics reported in Table 1.

2.1.2. Interpretability and Post-hoc Explanation Results

Global Shapley feature importance for g^{MGBM} on the mortgage test data is reported in Figure 1. g^{MGBM} places high importance on LTV ratio, perhaps too high, and also weighs DTI ratio, property value, loan amount, and introductory rate period heavily in many of its predictions.

**Figure 1.** Global mean absolute Tree SHAP feature importance for $g^{\text{MGBM}}(\mathbf{X})$ on the mortgage test data.

The potential over-emphasis of LTV ratio, and the de-emphasis of income, likely an important feature from a business perspective, and the encoded no introductory rate period flag feature may contribute to the decreased performance of g^{MGBM} as compared to g^{XNN} .

Domain knowledge was used to positively constrain DTI ratio and LTV ratio and to negatively constrain income and the loan term flag under g^{MGBM} . The monotonicity constraints for DTI ratio and LTV ratio are confirmed for $g^{\text{MGBM}}(\mathbf{X})$ on the mortgage test data in Figure 2. Both DTI ratio and LTV ratio display positive monotonic behavior at all selected percentiles for ICE and on average with PD. Because PD curves generally follow the patterns of the ICE curves for both features, it's also likely that no strong interactions are at play for DTI ratio and LTV ratio under g^{MGBM} . Of course, the monotonicity constraints themselves can dampen the effects of non-monotonic interactions under g^{MGBM} , even if they do exist in the data, and perhaps due to less noise in the mortgage data, this rigidity could also play a role in the performance differences between g^{MGBM} and g^{XNN} in the mortgage data. DTI ratio and LTV ratio also appear to have sparse regions in their univariate distributions. The monotonicity constraints likely play to the advantage of g^{MGBM} in this regard, as g^{MGBM} appears to carry reasonable predictions learned from populous domains into the sparse domains of both features.

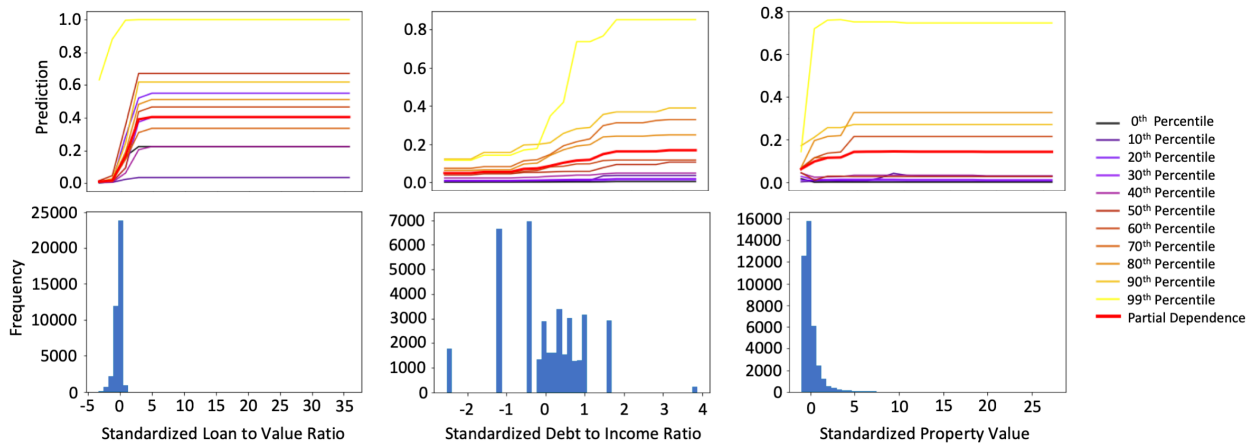


Figure 2. PD, ICE for 10 individuals across selected percentiles of $g^{\text{MGBM}}(\mathbf{X})$, and histograms for the three most important input features of g^{MGBM} on the mortgage test data.

Figure 2 also displays PD and ICE for the unconstrained feature property value. Unlike DTI ratio and LTV ratio, PD for property value does not always follow the patterns established by ICE curves. While PD shows monotonically increasing prediction behavior on average, apparently influenced by large predictions at extreme $g^{\text{MGBM}}(\mathbf{X})$ percentiles, ICE curves for individuals at the 40th percentile of $g^{\text{MGBM}}(\mathbf{X})$, and lower, exhibit different prediction behavior with respect to property value. Some individuals at these lower percentiles display monotonically decreasing prediction behavior while others appear to show fluctuating prediction behavior. Property value is strongly right-skewed, with little data regarding high-value property from which g^{MGBM} can learn. For the most part, reasonable predictions do appear to be carried from more densely populated regions to more sparsely populated regions. However, prediction fluctuations at lower $g^{\text{MGBM}}(\mathbf{X})$ percentiles are visible, and appear in a sparse region of property value. This divergence of PD and ICE can be indicative of an interaction affecting property value under g^{MGBM} [22], and analysis by surrogate decision tree did show evidence of numerous potential interactions in lower predictions ranges of $g^{\text{MGBM}}(\mathbf{X})$ [31] (not shown, but available in resources discussed in Subsection 1.8). However, fluctuations in ICE can also be caused by overfitting or leakage of strong non-monotonic signal from important constrained features into the modeled behavior of non-constrained features.

In Figure 3, local Tree SHAP values are displayed for selected individuals at the 10th, 50th, and 90th percentiles of $g^{\text{MGBM}}(\mathbf{X})$ in the mortgage test data. The selected individuals show an expected progression of mostly negative Shapley values at the 10th percentile, a mixture of positive and negative Shapley values at the 50th percentile, mostly positive Shapley values the 90th percentile, and with globally important features driving most local model decisions.

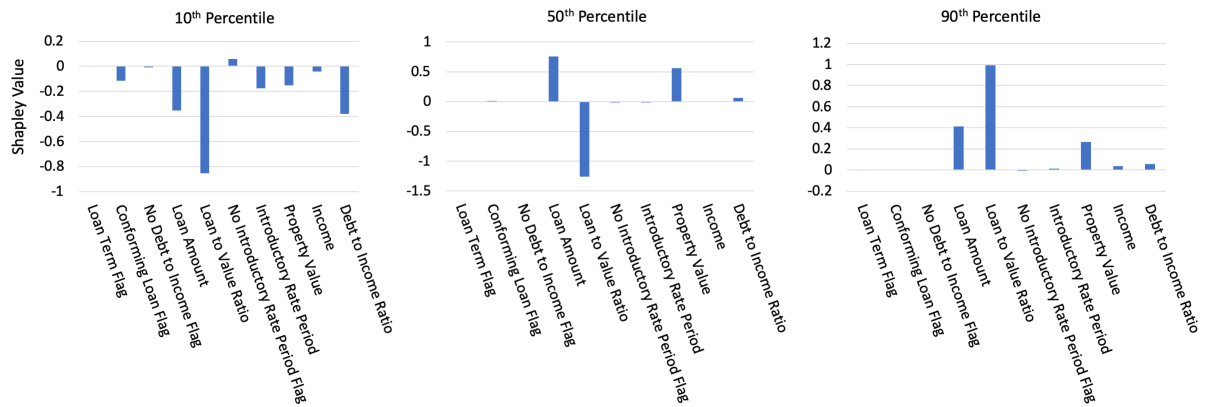


Figure 3. Tree SHAP values for three individuals across selected percentiles of $g^{\text{MGBM}}(\mathbf{X})$ for the mortgage test data.

Deeper significance for Figure 3 lies in the ability of Tree SHAP to accurately summarize any single $g^{\text{MGBM}}(\mathbf{x})$ prediction in this manner, which is generally important for enabling logical appeal or override of ML-based decisions, and is specifically important in the context of lending, where applicable regulations often require lenders to provide consumer-specific reasons for denying credit to an individual. In the US, applicable regulations are typically ECOA and FCRA, and the consumer-specific reasons are commonly known as adverse actions codes.

Figure 4 displays global feature importance for g^{XNN} on the mortgage test data. g^{XNN} distributes importance more evenly across business drivers and puts stronger emphasis on the no introductory rate period flag feature than does g^{MGBM} . Like g^{MGBM} , g^{XNN} puts little emphasis on the other flag features.

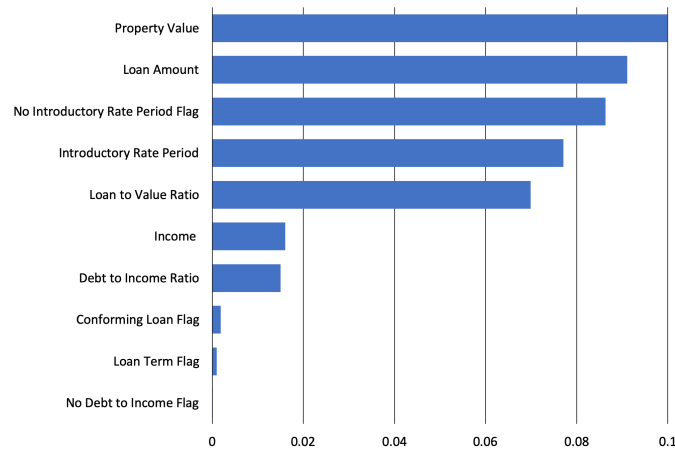


Figure 4. Global mean absolute Deep SHAP feature importance for $g^{\text{XNN}}(\mathbf{X})$ on the mortgage test data.

As compared to g^{MGBM} , g^{XNN} assigns higher importance to property value, loan amount, and income, and lower importance on LTV ratio and DTI ratio.

The capability of g^{XNN} to model nonlinear phenomenon and high-degree interactions, and to do so in an interpretable manner, is on display in Figure 5. 5 A presents the sparse γ_k weights of the g^{XNN} output layer in which the n_k subnetworks with $k \in \{0, 1, 2, 3, 5, 8, 9\}$ have large magnitude weights and n_k subnetworks, $k \in \{4, 6, 7\}$, have small or near-zero magnitude weights. Distinctive ridge functions that feed into those large magnitude γ_k weights are highlighted in 5 B and color-coded to pair with their corresponding γ_k weight. As in the subsection E.2, n_k ridge function plots vary with the output of the corresponding projection layer $\sum_j \beta_{k,j} x_j$ hidden unit, with weights displayed in matching colors in 5 C. In both the simulated and mortgage data, g^{XNN} n_k ridge functions appear to be elementary

functional forms that the output layer learns to combine to generate accurate predictions, reminiscent of basis functions for the modeled space.

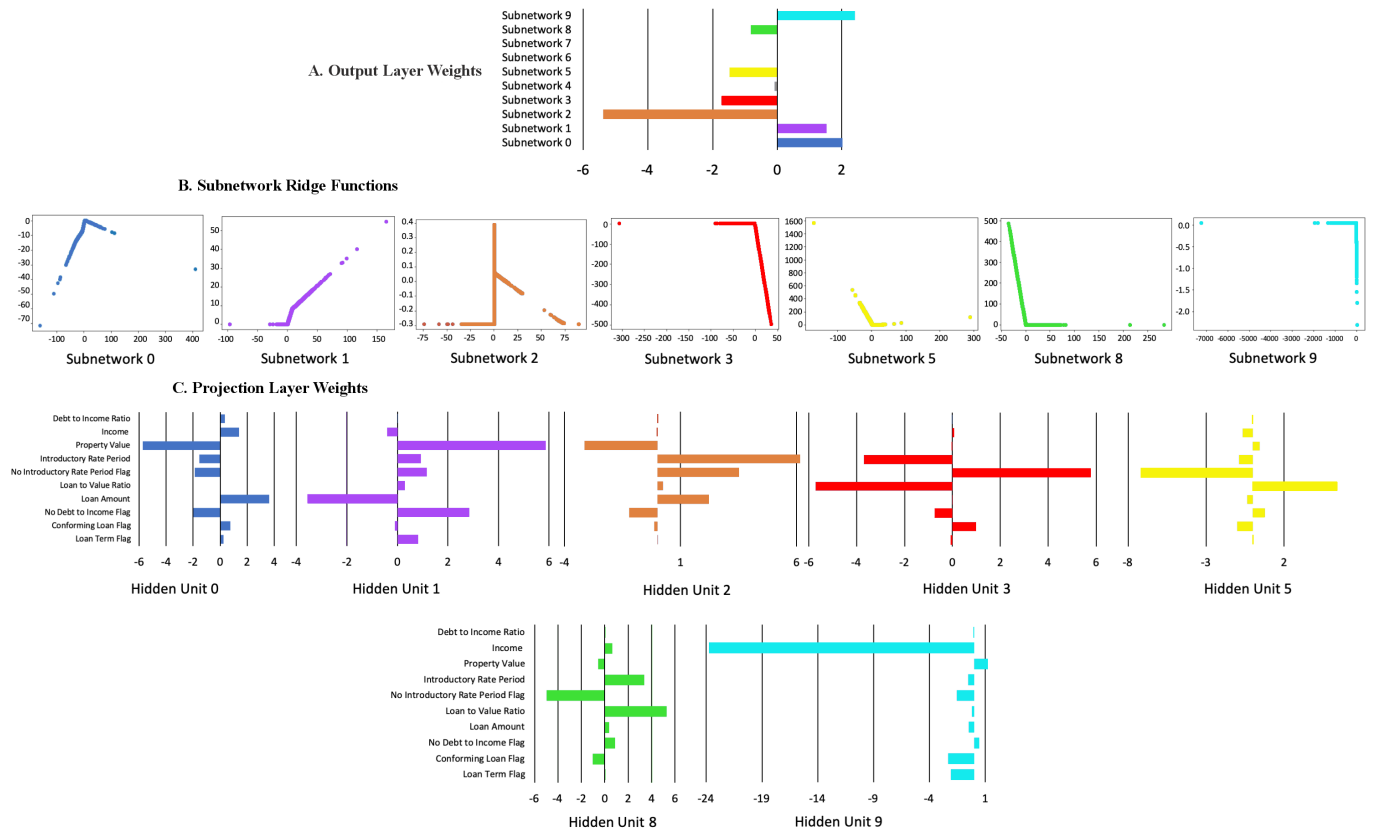


Figure 5. A. Output layer γ_k weights, B. corresponding n_k ridge functions, and C. associated projection layer β_j weights for g^{XNN} on the mortgage test data.

5 C displays the sparse β_j weights of the projection layer $\sum_j \beta_{k,j} x_j$ hidden units that are associated with
 287 each n_k subnetwork ridge function. For instance, subnetwork n_3 is influenced by large weights for
 288 LTV ratio, no introductory rate period flag, and introductory rate period, whereas subnetwork n_9 is
 289 nearly completely dominated by the weight for income.

To compliment the global interpretability of g^{XNN} , Figure 6 displays local Shapley values for
 291 selected individuals, estimated from the projection layer using Deep SHAP in the g^{XNN} probability
 292 space.

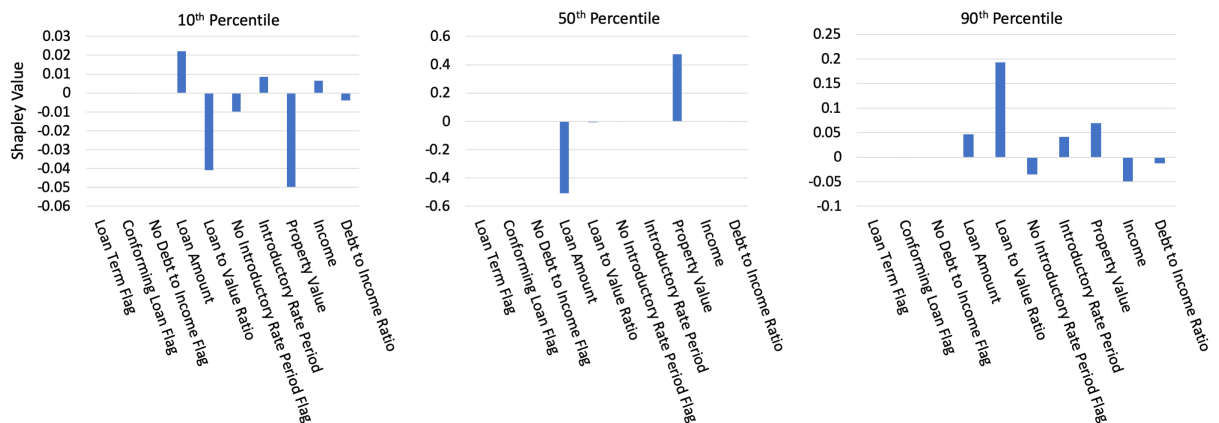


Figure 6. Deep SHAP values for three individuals across selected percentiles of $g^{\text{XNN}}(\mathbf{X})$ on the mortgage test data.

While the Shapley values appear to follow the roughly increasing pattern established in Figures A3, A6, and 3 their true value is their ability to be calculated for any $g^{XNN}(x)$ prediction, as a means to summarize model reasoning and allow for appeal and override of specific ML-based decisions, even for neural network architectures.

2.1.3. Discrimination Testing Results

Tables 2a and 2b show the results of the discrimination tests using the mortgage data for two sets of class-control groups: blacks as compared to whites, and females as compared to males. As with the simulated data, several measures of disparities are shown, with the SMDs calculated using the probabilities from g^{MGBM} and g^{XNN} , and the FPRs, FNRs, their ratios, MEs, and AIRs calculated using a binary outcome based on a cutoff of 0.20 (anyone with probabilities of 0.2 or less receives the favorable outcome). Since g^{MGBM} and g^{XNN} are predicting the likelihood of receiving a high-priced loan, g^{MGBM} and g^{XNN} assume that a lower score is favorable. Thus, one might consider FPR ratios as a measure of the class-control disparities. FPR ratios are higher under g^{XNN} than g^{MGBM} (2.45 vs. 2.10) in Table 2b, but overall FPRs are lower for blacks under g^{XNN} (0.295 vs. 0.315) in Table 2a. This is the same pattern seen in the simulated data results in Section E.3, again leading to the question of whether a fairness goal should not only consider class-control relative rates, but also intra-class improvements in the chosen fairness metric. Similar results are found for the female-male comparison, but the relative rates are less stark: 1.15 for g^{MGBM} and 1.21 for g^{XNN} .

(a) Group size, accuracy, and FNR for g^{MGBM} and g^{XNN} on the mortgage test data.

Class	N	Model	Accuracy	FNR
Black	2,608	g^{MGBM}	0.654	0.457
		g^{XNN}	0.702	0.308
White	28,361	g^{MGBM}	0.817	0.508
		g^{XNN}	0.857	0.360
Female	8,301	g^{MGBM}	0.768	0.402
		g^{XNN}	0.822	0.322
Male	13,166	g^{MGBM}	0.785	0.497
		g^{XNN}	0.847	0.347

(b) AIR, ME, SMD, and FNR ratio for g^{MGBM} and g^{XNN} on the mortgage test data.

Model	Protected Class	Control Class	AIR	ME	SMD	FNR Ratio
g^{MGBM}	Black	White	0.776	18.3%	0.628	0.900
	Female	Male	0.948	4.1%	0.084	0.810
g^{XNN}	Black	White	0.743	21.4%	0.621	0.855
	Female	Male	0.955	3.6%	0.105	0.927

Table 2. Discrimination measures for the mortgage test data.

Both ME and AIR show higher disparities for blacks under g^{XNN} than g^{MGBM} . Blacks receive high-priced loans 21.4% more frequently using g^{XNN} vs. 18.3% for g^{MGBM} . Both g^{MGBM} and g^{XNN} show AIRs that are statistically significantly below parity (not shown, but available in resources discussed in Subsection 1.8), and which are also below the EEOC's 0.80 threshold. This would typically indicate cause for further review to determine the cause and validity of these disparities, and a few relevant remediation techniques for such discovered discrimination are discussed in Section 3.3. On the other hand, women improve under g^{XNN} vs. g^{MGBM} (MEs of 3.6% vs. 4.1%; AIRs of 0.955 vs. 0.948). The AIRs, while statistically significantly below parity, are well above the EEOC's threshold of 0.80. In most situations, the values of these metrics alone would not likely flag a model for further review, though there may be other considerations which would lead to concern.

Black SMDs for g^{XNN} and g^{MGBM} are similar: 0.621 and 0.628, respectively. These exceed Cohen's guidelines of 0.5 for a medium effect size and would likely trigger further review. Female SMDs are well below Cohen's definition of small effect size: 0.105 and 0.084 for g^{XNN} and g^{MGBM} , respectively. Similar to results for female AIR, these values alone are unlikely to prompt further review.

3. Discussion

3.1. The Burgeoning Python Ecosystem for Responsible Machine Learning

Figure 7 displays a holistic approach to ML model training, assessment, deployment meant to decrease discrimination, inaccuracy, privacy, and security risks for high-stakes, human-centered, or regulated ML applications.¹¹

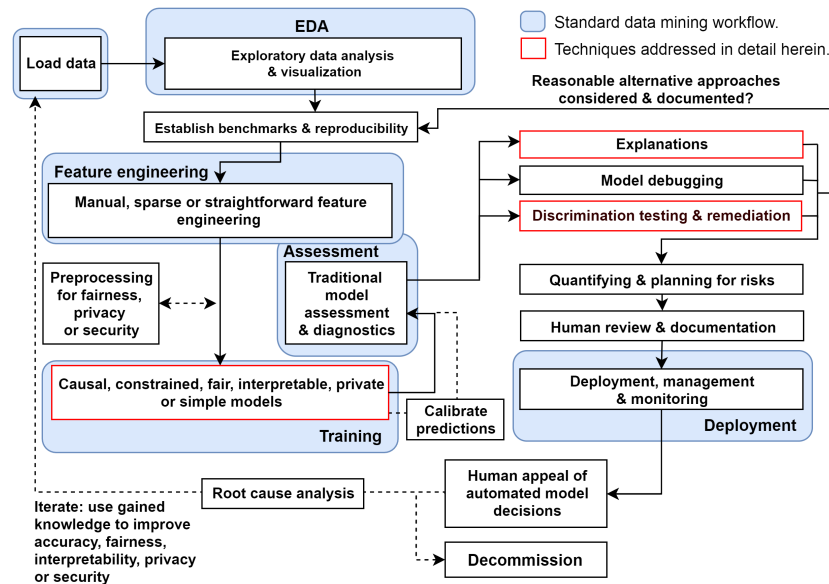


Figure 7. An example responsible ML workflow in which interpretable models, post-hoc explanations, discrimination testing and remediation techniques, among other review and appeal mechanisms, can create an understandable and trustworthy ML system.

While all the methods mentioned in Figure 7 play an important role in increasing human trust and understanding of ML, a few pertinent references and Python resources are highlighted below as further reading. Any discussion of interpretable ML models would be incomplete without references to the seminal work of the Rudin group at Duke University and EBM or GA²M models, pioneered by researchers at Microsoft and Cornell. In keeping with a major theme of this manuscript, models from these leading researchers and several other kinds of interpretable ML models are now available as open source Python packages. Among several types of currently available interpretable models, practitioners can now use Python to evaluate EBM in the `interpret` package, optimal sparse decision trees, GAMs in the `pyGAM` package, a variant of Friedman’s RuleFit in the `skope-rules` package, monotonic calibrated interpolated lookup tables in `tensorflow/lattice`, and *this looks like that* interpretable deep learning [32], [33], [34], [35].^{12,13} Additional, relevant references and Python functionality include:

- **Exploratory data analysis (EDA):** H2OAggregatorEstimator in `h2o` [36].
- **Sparse feature extraction:** H2OGeneralizedLowRankEstimator in `h2o` [37].
- **Privacy preprocessing and private models:** differential privacy and private models in `diffprivlib` and `tensorflow/privacy` [38], [39], [40], [41].
- **Post-hoc explanation:** structured data explanations with `alibi` and `PDPbox`, image classification explanations with `DeepExplain`, and natural language explanations with `allennlp` [42], [43], [44].
- **Discrimination testing:** with `aequitas` and `Themis`.

¹¹ See: [Toward Responsible Machine Learning](#) for details regarding Figure 7.

¹² See: [Optimal sparse decision trees](#).

¹³ See: [This looks like that interpretable deep learning](#).

- **Discrimination remediation:** Reweighting, adversarial de-biasing, learning fair representations, and reject option classification with [AIF360](#) [45], [46], [47], [48].
- **Model debugging:** with [foolbox](#), [SALib](#), [tensorflow/cleverhans](#), and [tensorflow/model-analysis](#) [49], [50], [51], [52].
- **Model documentation:** models cards [53], e.g., [GPT-2 model card](#), [Object Detection model card](#).

See: [Awesome Machine Learning Interpretability](#) for a longer, community-curated metalist of related software packages and resources.

3.2. Appeal and Override of Automated Decisions

Interpretable model architectures and post-hoc explanations play an important role in increasing transparency into model mechanisms and predictions. As seen in Sections 1 and 2, interpretable models often enable users to enforce domain knowledge-based constraints on model behavior, to ensure that models obey reasonable expectations, and to gain data-derived insights into the modeled problem domain. Post-hoc explanations generally help describe and summarize mechanisms and decisions, potentially yielding an even clearer understanding of ML models. Together they can allow for human learning from ML, certain types of regulatory compliance, and crucially, human appeal or override of automated model decisions [31]. Interpretable models and post-hoc explanations are likely good candidates for ML uses cases under the FCRA, ECOA, GDPR and other regulations that may require explanations of model decisions, and they are already used in the financial services industry today for model validation and other purposes.^{14,15} Writ large, transparency in ML also facilitates additional responsible AI processes such as model debugging, model documentation, and logical appeal and override processes, some of which may also be required by applicable regulations.¹⁶ Among these, providing people affected by a model with the opportunity to appeal ML-based decisions may deserve the most attention. ML models are often wrong¹⁷ and appealing black-box decisions is difficult.² For high-stakes, human-centered, or regulated applications that are trusted with mission- or life-critical decisions, the ability to logically appeal or override inevitable wrong decisions is not only a possible prerequisite for regulatory compliance, but also an important failsafe procedure for those affected by ML decisions.

3.3. Discrimination Testing and Remediation in Practice

The heightened interest in exploring and fixing algorithmic bias has led to a significant body of work focused in using ML to diminish discrimination in model outcomes [56]. Broadly, these can be defined into two groups: more traditional methods that mitigate discrimination by searching across possible algorithmic and feature specifications, and more recently developed approaches that change the algorithms or input data themselves in order to mitigate disparities. Many approaches that have been developed in the last five to seven years focus on altering the algorithm itself, preprocessing the data, or post-processing the predictions in order to diminish class-control correlations or dependencies. For comments on why these techniques could result in regulatory non-compliance in certain cases, see Appendix G.

Whether these methods are suitable for a particular use case depends on the legal environment in which the model will be used and the use case itself. Of the newer class of fairness enhancing

¹⁴ See: [Deep Insights into Explainability and Interpretability of Machine Learning Algorithms and Applications to Risk Management](#).

¹⁵ Unfortunately, many non-consistent explanation methods can result in drastically different global and local feature importance values across different models trained on the same data or even for refreshing a model with augmented training data [54]. Consistency and accuracy guarantees are perhaps a factor in the growing momentum behind Shapley values as a candidate technique for generating consumer-specific adverse action notices for explaining and appealing automated ML-based decisions in highly-regulated settings, such as credit lending [55].

¹⁶ E.g.: [US Federal Reserve Bank Supervision and Regulation \(SR\) Letter 11-7: Guidance on Model Risk Management](#).

¹⁷ "All models are wrong, but some are useful." – George Box, Statistician (1919 - 2013)

interventions in ML, within-algorithm discrimination mitigation techniques that do not use class information may be more likely to be acceptable in highly regulated settings today. These techniques work by incorporating a loss function where more discriminatory paths or weights are penalized and will only be used by the model if the increase in model performance overcomes the penalty (the relative level of performance-to-discrimination penalty is determined via a hyperparameter choice). Other mitigation strategies that only alter hyperparameters or algorithm choice are also likely to be acceptable. And feature selection techniques that have been used in traditional modeling (ordinary least squares, logistic, and simple decision tree models) are likely to continue to be accepted in regulatory environments. For further discussion of potential and utilized techniques that can mitigate disparate impact in financial services, see Schmidt and Stephens [57].

Regardless of the methodology chosen to minimize disparities, advances in computing have enhanced the ability to search for less discriminatory models. Prior to these advances, only a small number of alternative algorithms could be tested for lower levels of disparity without causing infeasible delays in model implementation. Now, tens of thousands of alternative models or more can be quickly tested for lower discrimination and better predictive quality. An additional opportunity arises as a result of ML itself: the well-known Rashomon effect, or the multiplicity of good ML models for most datasets. Thus, it is now feasible to train more models, find more good models, and test more models for discrimination, and among all those tested models, there are likely to be some with high predictive performance and low discrimination.

3.4. Intersectional and Non-static Problems in Machine Learning

The black-box nature of ML, the perpetuation or exacerbation of discrimination by ML, or the security vulnerabilities inherent in ML are each serious and difficult problems on their own. However, evidence is mounting that these harms can also manifest as complex intersectional challenges, e.g., the *fairwashing* or *scaffolding* of biased models with ML explanations, the privacy harms of ML explanations, or the adversarial poisoning of ML models to become discriminatory [8], [18], [19].^{18,19,20} Practitioners should of course consider the discussed interpretable modeling, post-hoc explanation, and discrimination testing approaches as at least partial remedies to the black-box and discrimination issues in ML. However, they should also consider that explanations can ease model stealing, data extraction, and membership inference attacks, and that explanations can mask ML discrimination. Additionally, high-stakes, human-centered, or regulated ML systems should generally be built and tested with robustness to adversarial attacks as a primary design consideration, and specifically to prevent ML models from being poisoned or otherwise altered to become discriminatory. Accuracy, discrimination, and security characteristics of a system can change over time as well. Simply testing for these problems at training time, as presented in Sections 1 and 2, is not adequate for high-stakes, human-centered, or regulated ML systems. Accuracy, discrimination, and security should be monitored in real-time and over time, as long as a model is deployed.

4. Conclusion

This text puts forward results on simulated data to provide a rough validation of constrained ML models, post-hoc explanation techniques, and discrimination testing methods. These same modeling, explanation, and discrimination testing approaches are then applied to more realistic mortgage data to provide an example of a responsible ML workflow for high-stakes, human-centered, or regulated

¹⁸ See: [Tay, Microsoft's AI chatbot, gets a crash course in racism from Twitter](#).

¹⁹ While the focus of this paper is not ML security, proposed best-practices from that field do point to transparency of ML systems as a mitigating factor for some ML attacks and hacks [52]. High system complexity is sometimes considered a mitigating influence as well [58]. This is sometimes known as the *transparency paradox* in data privacy and security, and it likely applies to ML security as well, especially in the context of interpretable ML models and post-hoc explanation.²⁶

²⁰ See: [The AI Transparency Paradox](#).

ML applications. The discussed methodologies are solid steps toward interpretability, explanation, and minimal discrimination for ML decisions, which should ultimately enable increased fairness and logical appeal processes for ML decision subjects. Of course, there is more to the responsible practice of ML than interpretable models, post-hoc explanation, and discrimination testing, even from a technology perspective, and Section 3 also points out numerous additional references and open source Python software assets that are available to researchers and practitioners today to increase human trust and understanding in ML systems. While the messy, complex, and human problems of racism, sexism, privacy violations, and cyber crime can probably not be solved by technology alone, this work (and many, many others) illustrate numerous ways for ML practitioners to become part of the solution to these problems, instead of perpetuating and exacerbating them.

Author Contributions: NG, data cleaning, GBM and MGBM assessment and results; PH, primary author; KM, ANN and XNN implementation, assessment, and results; NS, secondary author, data simulation and collection, and discrimination testing.

Funding: This work received no external funding.

Acknowledgments: Wen Phan for work in formalizing notation. Sue Shay for editing. Andrew Burt for ideas around the transparency paradox.

Conflicts of Interest: XNN was first made public by the corporate model validation team at Wells Fargo bank. Wells Fargo is a customer of, and investor in, H2O.ai and a client of BLDS, LLC. However, communications regarding XNN between Wells Fargo and the authors have been extremely limited prior to and during the drafting of this manuscript. Moreover, Wells Fargo exerted absolutely no editorial control over the text or results herein.

Abbreviations

The following abbreviations are used in this text: AI – artificial intelligence, AIR – adverse impact ratio, ALE – accumulated local effect, ANN – artificial neural network, APR – annual percentage rate, AUC – area under the curve, CNN – convolutional neural network, CFPB – Consumer Financial Protection Bureau, DI – disparate impact, DT – disparate treatment, DTI – debt to income, EBM or GA²M – explainable boosting machine, i.e. variants GAMs that consider two-way interactions and may incorporate boosting into training, EEOC – Equal Employment Opportunity Commission, ECOA – Equal Credit Opportunity Act, EDA – exploratory data analysis, EU – European Union, FCRA – Fair Credit Reporting Act, FNR – false negative rate, FPR – false positive rate, GAM – generalized additive model, GBM – gradient boosting machine, GDPR – General Data Protection Regulation, HMDA – Home Mortgage Disclosure Act, ICE – individual conditional expectation, LTV – loan to value, ME – marginal effect, MGBM – monotonic gradient boosting machine, ML – machine learning, PD – partial dependence, RMSE – root mean square error, SGD – stochastic gradient descent, SHAP – Shapley additive explanation, SMD – standardized mean difference, SR – supervision and regulation, US – United States, XNN – explainable neural network.

Appendix A. HMDA Mortgage Data Details

The US HMDA law, originally enacted in 1975, requires many financial institutions that originate mortgage products to provide certain data about many of the mortgage-related products that they either deny or originate on an annual basis. This information is first provided to the Consumer Financial Protection Bureau (CFPB), which subsequently releases some of the data to the public. Regulators often use HMDA data to, “...show whether lenders are serving the housing needs of their communities; they give public officials information that helps them make decisions and policies; and they shed light on lending patterns that could be discriminatory.”⁵ In addition to regulatory use, public advocacy groups use these data for similar purposes, and the lenders themselves use the data to benchmark their community outreach relative to their peers. The publicly available data that the CFPB releases includes information such as the lender, the type of loan, loan amount, loan to value (LTV) ratio, debt to income (DTI) ratio, and other important financial descriptors. The data also include information on each borrower and co-borrower’s race, ethnicity, gender, and age. Because the data includes information on these protected class characteristics, certain metrics that can be indicative of

discrimination in lending can be calculated directly using the HDMA data. Ultimately, the HDMA data represent the most comprehensive source of data on highly-regulated mortgage lending that is publicly available, which makes it an ideal dataset to use for the types of analyses set forth in Sections 1 and 2.

Appendix B. Selected Algorithmic Details

Appendix B.1. Notation

To facilitate descriptions of data and modeling, explanatory, and discrimination testing techniques, notation for input and output spaces, datasets, and models is defined.

Appendix B.1.1. Spaces

- Input features come from the set \mathcal{X} contained in a P -dimensional input space, $\mathcal{X} \subset \mathbb{R}^P$. An arbitrary, potentially unobserved, or future instance of \mathcal{X} is denoted \mathbf{x} , $\mathbf{x} \in \mathcal{X}$.
- Labels corresponding to instances of \mathcal{X} come from the set \mathcal{Y} .
- Learned output responses of models are contained in the set $\hat{\mathcal{Y}}$.

Appendix B.1.2. Datasets

- The input dataset \mathbf{X} is composed of observed instances of the set \mathcal{X} with a corresponding dataset of labels \mathbf{Y} , observed instances of the set \mathcal{Y} .
- Each i -th observation of \mathbf{X} is denoted as $\mathbf{x}^{(i)} = [x_0^{(i)}, x_1^{(i)}, \dots, x_{P-1}^{(i)}]$, with corresponding i -th labels in \mathbf{Y} , $\mathbf{y}^{(i)}$, and corresponding predictions in $\hat{\mathbf{Y}}$, $\hat{\mathbf{y}}^{(i)}$.
- \mathbf{X} and \mathbf{Y} consist of N tuples of observations: $[(\mathbf{x}^{(0)}, \mathbf{y}^{(0)}), (\mathbf{x}^{(1)}, \mathbf{y}^{(1)}), \dots, (\mathbf{x}^{(N-1)}, \mathbf{y}^{(N-1)})]$.
- Each j -th input column vector of \mathbf{X} is denoted as $X_j = [x_j^{(0)}, x_j^{(1)}, \dots, x_j^{(N-1)}]^T$.

Appendix B.1.3. Models

- A type of ML model g , selected from a hypothesis set \mathcal{H} , is trained to represent an unknown signal-generating function f observed as \mathbf{X} with labels \mathbf{Y} using a training algorithm \mathcal{A} : $\mathbf{X}, \mathbf{Y} \xrightarrow{\mathcal{A}} g$, such that $g \approx f$.
- g generates learned output responses on the input dataset $g(\mathbf{X}) = \hat{\mathbf{Y}}$, and on the general input space $g(\mathcal{X}) = \hat{\mathcal{Y}}$.
- The model to be explained and tested for discrimination is denoted as g .

Appendix B.2. Monotonic Gradient Boosting Machine

MGBMs constrain typical GBM training to consider only tree splits that obey user-defined positive and negative monotonicity constraints, with respect to each X_j and \mathbf{y} independently. The MGBM remains an additive combination of B trees trained by gradient boosting, T_b , and each tree learns a set of splitting rules that respect monotonicity constraints, Θ_b^{mono} .

$$g^{\text{MGBM}}(\mathbf{x}) = \sum_{b=1}^B T_b(\mathbf{x}; \Theta_b^{\text{mono}}) \quad (\text{A1})$$

As in unconstrained GBM, Θ_b^{mono} is selected in a greedy, additive fashion by minimizing a regularized loss function that considers known target labels, \mathbf{y} , the predictions of all subsequently trained trees in the in $g^{\text{MGBM}}, g_{b-1}^{\text{MGBM}}(\mathbf{X})$, and the b -th tree splits, $T_b(\mathbf{x}^{(i)}; \Theta_b^{\text{mono}})$, in a numeric error function (e.g., squared error, Huber error), l , and a regularization term that penalizes complexity in the current tree, $\Omega(T_b)$. For the b -th iteration, the loss function, \mathcal{L}_b , can generally be defined as:

$$\mathcal{L}_b = \sum_{i=0}^{N-1} l(y^{(i)}, g_{b-1}^{\text{MGBM}}(\mathbf{x}^{(i)}) + T_b(\mathbf{x}^{(i)}; \Theta_b^{\text{mono}})) + \Omega(T_b) \quad (\text{A2})$$

513 In addition to \mathcal{L}_b , g^{MGBM} training is characterized by additional splitting rules and constraints on
 514 tree node weights. Each binary splitting rule, $\theta_{b,j,k} \in \Theta_b$, is associated with a feature, X_j , is the
 515 k -th split associated with X_j in T_b , and results in left and right child nodes with a numeric weights,
 516 $\{w_{b,j,k,L}, w_{b,j,k,R}\}$. For terminal nodes, $\{w_{b,j,k,L}, w_{b,j,k,R}\}$ can be direct numeric components of some
 517 g^{MGBM} prediction. For two values of some feature X_j , $x_j^\alpha \leq x_j^\beta$, g^{MGBM} is positive monotonic with
 518 respect to some X_j if $g^{\text{MGBM}}(x_j^\alpha) \leq g^{\text{MGBM}}(x_j^\beta) \forall x_j^\alpha \leq x_j^\beta \in X_j$. The following rules and constraints
 519 ensure positive monotonicity in Θ_b , where the prediction for each value results in $T_b(x_j^\alpha; \Theta_b) = w_\alpha$
 520 and $T_b(x_j^\beta; \Theta_b) = w_\beta$.

- 521 1. For the first and highest split in T_b involving X_j , any $\theta_{b,j,0}$ resulting in $T(x_j; \theta_{b,j,0}) =$
 522 $\{w_{b,j,0,L}, w_{b,j,0,R}\}$ where $w_{b,j,0,L} > w_{b,j,0,R}$, is not considered.
- 523 2. For any subsequent left child node involving X_j , any $\theta_{b,j,k \geq 1}$ resulting in $T(x_j; \theta_{b,j,k \geq 1}) =$
 524 $\{w_{b,j,k \geq 1,L}, w_{b,j,k \geq 1,R}\}$ where $w_{b,j,k \geq 1,L} > w_{b,j,k \geq 1,R}$, is not considered.
- 525 3. Moreover, for any subsequent left child node involving X_j , $T(x_j; \theta_{b,j,k \geq 1}) = \{w_{b,j,k \geq 1,L}, w_{b,j,k \geq 1,R}\}$,
 526 $\{w_{b,j,k \geq 1,L}, w_{b,j,k \geq 1,R}\}$ are bound by the associated $\theta_{b,j,k-1}$ set of node weights,
 527 $\{w_{b,j,k-1,L}, w_{b,j,k-1,R}\}$, such that $\{w_{b,j,k \geq 1,L}, w_{b,j,k \geq 1,R}\} < \frac{w_{b,j,k-1,L} + w_{b,j,k-1,R}}{2}$.
- 528 4. (1) and (2) are also applied to all right child nodes, except that for right child nodes $w_{b,j,k,L} \leq$
 529 $w_{b,j,k,R}$ and $\{w_{b,j,k \geq 1,L}, w_{b,j,k \geq 1,R}\} \geq \frac{w_{b,j,k-1,L} + w_{b,j,k-1,R}}{2}$.

530 Note that for any one X_j and $T_b \in g^{\text{MGBM}}$ left subtrees will always produce lower predictions than
 531 right subtrees, and that any $g^{\text{MGBM}}(\mathbf{x})$ is an addition of each T_b output, with the application of
 532 a monotonic logit or softmax link function for classification problems. Moreover, each tree's root
 533 node corresponds to some constant node weight that by definition obeys monotonicity constraints,
 534 $T(x_j^\alpha; \theta_{b,0}) = T(x_j^\beta; \theta_{b,0}) = w_{b,0}$. Together these additional splitting rules and node weight constraints
 535 ensure that $g^{\text{MGBM}}(x_j^\alpha) \leq g^{\text{MGBM}}(x_j^\beta) \forall x_j^\alpha \leq x_j^\beta \in X_j$. For a negative monotonic constraint, i.e.,
 536 $g^{\text{MGBM}}(x_j^\alpha) \geq g^{\text{MGBM}}(x_j^\beta) \forall x_j^\alpha \leq x_j^\beta \in X_j$, left and right splitting rules and node weight constraints are
 537 switched. Also consider that MGBM models with independent monotonicity constraints between some
 538 X_j and \mathbf{y} likely restrict non-monotonic interactions between multiple X_j . Moreover, if monotonicity
 539 constraints are not applied to all $X_j \in \mathbf{X}$, any strong non-monotonic signal in training data associated
 540 with some important X_j maybe forced onto some other arbitrary unconstrained X_j under some g^{MGBM}
 541 models, compromising the end goal of interpretability.

542 Appendix B.3. Explainable Neural Network

543 XNNs are an alternative formulation of additive index models in which the ridge functions are
 544 neural networks [20]. XNNs also bear a strong resemblance to generalized additive models (GAMs)
 545 and so-called explainable boosting machines (EBMs or GA²M), i.e., GAMs which consider main
 546 effects and a small number of 2-way interactions and may also incorporate boosting into their training
 547 [13], [28]. Hence, XNNs enable users to tailor interpretable neural network architectures to a given
 548 prediction problem and to visualize model behavior by plotting ridge functions. XNNs are composed
 549 of a global bias term, μ_0 , K individually specified neural networks, n_k with scale parameters γ_k , and
 550 the inputs to each n_k are themselves a linear combination of modeling inputs, $\sum_j \beta_{k,j} x_j$.

$$551 \quad g^{\text{XNN}}(\mathbf{x}) = \mu_0 + \sum_{k=0}^{K-1} \gamma_k n_k \left(\sum_{j=0}^{J=P-1} \beta_{k,j} x_j \right) \quad (\text{A3})$$

551 g^{XNN} is comprised of 3 meta-layers:

- 552 1. The first and deepest meta-layer, composed of K linear $\sum_j \beta_{k,j} x_j$ hidden units, which should learn
 553 higher magnitude weights for important X_j , is known as the *projection layer*. It is fully connected
 554 to each input X_j . Each hidden unit in the projection layer may optionally include a bias term.

2. The second meta-layer contains K hidden and separate n_k ridge functions, or *subnetworks*. Each n_k is a neural network, which can be parameterized to suit a given modeling task. To facilitate direct interpretation and visualization, the input to each subnetwork is the 1-dimensional output of its associated projection layer hidden unit, $\sum_j \beta_{k,j} x_j$. Each n_k can contain several bias terms.
3. The output meta-layer, called the *combination layer*, is another linear unit comprised of a global bias term, μ_0 , and the K weighted 1-dimensional outputs of each subnetwork, $\gamma_k n_k(\sum_j \beta_{k,j} x_j)$. Again, subnetwork output is restricted to 1-dimension for interpretation and visualization purposes.

Appendix B.4. One-dimensional Partial Dependence and Individual Conditional Expectation

Following Friedman *et al.* [13] a single feature $X_j \in \mathbf{X}$ and its complement set $\mathbf{X}_{\mathcal{P} \setminus \{j\}} \in \mathbf{X}$ (where $X_j \cup \mathbf{X}_{\mathcal{P} \setminus \{j\}} = \mathbf{X}$) is considered. $\text{PD}(X_j, g)$ for a given feature X_j is estimated as the average output of the learned function $g(\mathbf{X})$ when all the observations of X_j are set to a constant $x \in \mathcal{X}$ and $\mathbf{X}_{\mathcal{P} \setminus \{j\}}$ is left unchanged. $\text{ICE}(x_j, \mathbf{x}, g)$ for a given instance \mathbf{x} and feature x_j is estimated as the output of $g(\mathbf{x})$ when x_j is set to a constant $x \in \mathcal{X}$ and all other features $\mathbf{x} \in \mathbf{X}_{\mathcal{P} \setminus \{j\}}$ are left untouched. PD and ICE curves are usually plotted over some set of constants $x \in \mathcal{X}$, as displayed in Section 2. Due to known problems for PD in the presence of strong correlation and interactions, PD should not be used alone. PD should be paired with ICE or be replaced with accumulated local effect (ALE) plots [22], [29].

Appendix B.5. Shapley Values

For some instance $\mathbf{x} \in \mathcal{X}$, Shapley explanations take the form:

$$g(\mathbf{x}) = \phi_0 + \sum_{j=0}^{j=\mathcal{P}-1} \phi_j \mathbf{z}_j \quad (\text{A4})$$

In Equation A4, $\mathbf{z} \in \{0, 1\}^{\mathcal{P}}$ is a binary representation of \mathbf{x} where 0 indicates missingness. Each ϕ_j is the local feature contribution value associated with x_j and ϕ_0 is the average of $g(\mathbf{X})$. Each ϕ_j is a weighted combination of model scores, $g_x(\mathbf{x})$, with x_j , $g_x(S \cup \{j\})$, and the model scores without x_j , $g_x(S)$, for every subset of features S not including j , $S \subseteq \mathcal{P} \setminus \{j\}$, where g_x incorporates the mapping between \mathbf{x} and the binary vector \mathbf{z} .

$$\phi_j = \sum_{S \subseteq \mathcal{P} \setminus \{j\}} \frac{|S|!(\mathcal{P} - |S| - 1)!}{\mathcal{P}!} [g_x(S \cup \{j\}) - g_x(S)] \quad (\text{A5})$$

Local, per-instance explanations using Shapley values tend to involve ranking x_j by ϕ_j values or delineating a set of the X_j names associated with the k -largest ϕ_j values for some \mathbf{x} , where k is some small positive integer, say 5. Global explanations are typically the absolute mean of the ϕ_j associated with a given X_j across all of the observations in some set \mathbf{X} .

Appendix C. Machine Learning Discrimination Under US Law

Before discussing the techniques, it is important to explain and draw a distinction between the two major types of discrimination recognized in US legal and regulatory settings, disparate treatment (DT), and disparate impact (DI). DT (which is loosely referred to as *intentional discrimination*) occurs most often in an algorithmic setting when a model explicitly uses protected class status (e.g., race, sex) as an input feature or uses a feature that is so similar to protected class status that it essentially proxies for class membership. With some limited exceptions, the use of these factors in an algorithm is illegal under several statutes in the US.⁴ DI, colloquially known as *unintentional discrimination*, occurs when some element of a decisioning process includes a *facially neutral* factor (i.e., a reasonable and valid predictor of response) that results in a disproportionate share of a protected class receiving an unfavorable outcome. In modeling, this is most typically driven by a statistically important feature that is distributed unevenly across classes, which causes more frequent unfavorable outcomes for the protected class. However, other factors, such as hyperparameter or algorithm choices, can drive

DI. Crucially, legality hinges on whether changing the model, for example exchanging one feature for another or altering the hyperparameters of an algorithm, can lead to a similarly predictive model with lower disparate impact. The analyses and metrics herein focus on several measures of disparate impact that are commonly used in US litigation and regulatory settings.

Appendix D. Practical vs. Statistical Significance for Discrimination Metrics

A finding of *practical significance* means the disparity found is not only statistically significant, but also passes beyond a chosen threshold that would constitute *prima facie* evidence of illegal discrimination. Its use represents a recognition that any large dataset is likely to show statistically significant differences in outcomes by class, even if those differences are not truly meaningful. It further recognizes that there are likely to be situations where differences in outcomes are beyond a model user's ability to correct them without significantly degrading the quality of the model. Moreover, practical significance is also needed by model builders and compliance personnel to determine whether a model should undergo remediation efforts before it is put into production. Unfortunately, guidelines for practical significance, i.e., the threshold at which any statistically significant disparity would be considered evidence of illegal discrimination, are not as frequently codified as the standards for statistical significance. One exception, however, is in employment discrimination analyses, where the US Equal Employment Opportunity Commission (EEOC) has stated that if the AIR is below 0.80 and statistically significant, then this constitutes *prima facie* evidence of discrimination, which the model user must rebut in order for the disparate impact not to be considered illegal discrimination.²¹ It is important to note that the 0.80 measure of practical significance, also known as the *80% rule* and the *4/5ths rule*, is explicitly used in relation to AIR, and it is not clear that the use of this threshold is directly relevant to testing fairness for metrics other than the AIR.

The legal thresholds for determining statistical significance is clearer and more consistent than that for practical significance. The first guidance in US courts occurred in a case involving discrimination in jury selection, *Castaneda v. Partida*.²² Here, the US Supreme Court wrote that, "As a general rule for such large samples, if the difference between the expected value and the observed number is greater than two or three standard deviations, then the hypothesis that the jury drawing was random would be suspect to a social scientist." This "two or three standard deviations" test was then applied to employment discrimination in *Hazelwood School Districts v. United States*.²³ Out of this, a 5% two-sided test ($z=1.96$), or an equivalent 2.5% one-sided test, has become a common standard for determining whether evidence of disparities is statistically significant.

Appendix E. Simulated Data Results

Model fit is roughly uniform for g^{GBM} , g^{MGBM} , g^{ANN} , and g^{XNN} on the simulated test data. Given that little or no trade-off is required in terms of model to fit to use the constrained models, intrinsic interpretability, post-hoc explainability, and discrimination are explored further for the g^{MGBM} and g^{XNN} models in Sections E.2 - E.3. For g^{MGBM} , intrinsic interpretability is evaluated with PD and ICE plots of mostly monotonic prediction behavior for several important X_j , and post-hoc Shapley explanation analysis is used to create global and local feature importance. For g^{XNN} , inherent interpretability manifests as plots of sparse γ_k output layer weights, n_k subnetwork ridge functions, and sparse β_j weights in the projection layer. Post-hoc Shapley explanation techniques are also used to generate global and local feature importance for g^{XNN} . Both g^{MGBM} and g^{XNN} are evaluated for discrimination using AIR, ME, SMD, and other measures.

²¹ Importantly, the standard of 0.80 is not a law, but a rule of thumb for agencies tasked with enforcement of discrimination laws. "Adoption of Questions and Answers To Clarify and Provide a Common Interpretation of the Uniform Guidelines on Employee Selection Procedures," Federal Register, Volume 44, Number 43 (1979).

²² *Castaneda v. Partida*, 430 US 482 - Supreme Court (1977)

²³ *Hazelwood School Dist. v. United States*, 433 US 299 (1977)

Appendix E.1. Constrained vs. Unconstrained Model Fit Assessment

Table A1 presents a variety of fit metrics for the g^{GBM} , g^{MGBM} , g^{ANN} , and g^{XNN} on the simulated test data. g^{GBM} exhibits the best performance, but all models give relatively similar fit results.

Table A1. Fit metrics for g^{GBM} , g^{MGBM} , g^{ANN} , and g^{XNN} on the simulated test data.

Model	Accuracy	AUC	Logloss	RMSE
g^{GBM}	0.775	0.857	0.474	0.394
g^{MGBM}	0.763	0.846	0.498	0.405
g^{ANN}	0.757	0.850	0.480	0.398
g^{XNN}	0.758	0.851	0.479	0.397

Interpretability and explainability benefits of the constrained models appear to come at little cost to overall model performance, or in the case of g^{ANN} and g^{XNN} , no cost at all. g^{XNN} actually shows slightly better fit than g^{ANN} across accuracy, area under the curve (AUC), logloss, and root mean squared error (RMSE). Accuracy is measured at the best F1 threshold for each model.

Appendix E.2. Interpretability and Post-hoc Explanation Results

Global mean absolute Shapley value feature importance for $g^{\text{MGBM}}(\mathbf{X})$ on the simulated test data is displayed in Figure A1. Tree SHAP values are reported in the margin space, prior to the application of the logit link function, and the reported numeric values can be interpreted as the mean absolute impact of each X_j on $g^{\text{MGBM}}(\mathbf{X})$ in the simulated test data in the g^{MGBM} margin space.

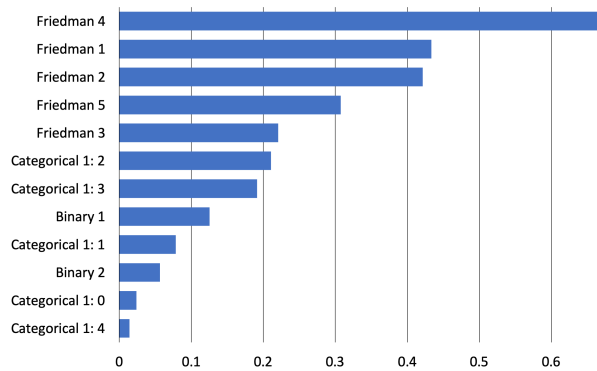


Figure A1. Global mean absolute Tree SHAP feature importance for $g^{\text{MGBM}}(\mathbf{X})$ on the simulated test data.

As expected, the $X_{\text{Friedman},j}$ features from the original Friedman [10] and Friedman *et al.* [11] formula are the main drivers of $g^{\text{MGBM}}(\mathbf{X})$ predictions, with encoded versions of the augmented categorical and binary features contributing less on average to $g^{\text{MGBM}}(\mathbf{X})$ predictions.

Figure A2 highlights PD, ICE, and histograms of the most important features from Figure A1. PD gives an indication of the estimated average prediction of $g^{\text{MGBM}}(\mathbf{X})$ in the test data for some X_j . ICE serves several purposes. It indicates the trustworthiness of the PD in the presence of interactions and correlation, it can be an interaction detector, and is also a type of sensitivity analysis where certain X_j are varied in single records under g^{MGBM} to provide a glimpse at local model behavior. PD and ICE are displayed with a histogram in Section 2 to highlight any sparse regions in an input feature's domain. Because most ML models will always issue a prediction on any datum with a correct schema, it's crucial to consider whether a given model learned enough about an observation to make an accurate prediction. Viewing PD and ICE along with a histogram is a convenient method to visually assess whether a prediction is reasonable and based on sufficient training data.

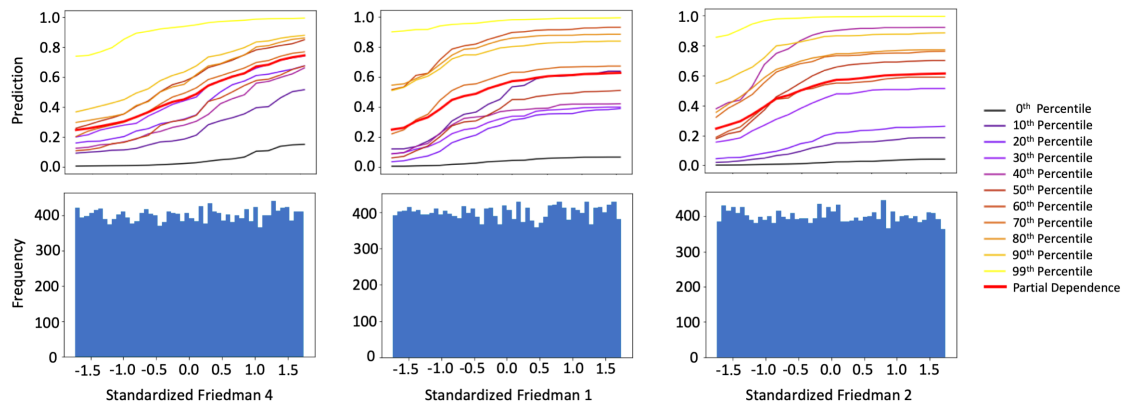


Figure A2. PD, ICE for 10 observations across selected percentiles of $g^{\text{MGBM}}(\mathbf{X})$, and histograms for the three most important input features of g^{MGBM} on the simulated test data.

$X_{\text{Friedman},1}$, $X_{\text{Friedman},2}$, and $X_{\text{Friedman},4}$ were positively monotonically constrained under g^{MGBM} for the simulated data, and positive monotonicity looks to be confirmed on average with PD and at numerous local percentiles of $g^{\text{MGBM}}(\mathbf{X})$ with ICE. Also, as the PD curves generally follow the patterns of the ICE curves, PD is likely an accurate representation of average feature behavior for $X_{\text{Friedman},1}$, $X_{\text{Friedman},2}$, and $X_{\text{Friedman},4}$. Since PD and ICE curves do not obviously diverge, g^{MGBM} is probably not modeling strong interactions, despite the fact that known interactions are included in the simulated data signal generating function in Equation 1. The one-dimensional monotonic constraints may hinder the modeling of such interactions, but do not strongly affect overall g^{MGBM} accuracy, perhaps due to noise in the simulated data. This is an interesting result for responsible ML practitioners. In some noisy scenarios, monotonicity constraints can increase model interpretability without causing a drastic drop in model accuracy, even when known interactions and non-monotonic behavior exist in training data.

Local Shapley values for records at the 10th, 50th, and 90th percentiles of $g^{\text{MGBM}}(\mathbf{X})$ in the simulated test data are displayed in Figure A3. These Tree SHAP values are reported in the margin space of g^{MGBM} , and each ϕ_j value in Figure A3 represents the difference in $g^{\text{MGBM}}(\mathbf{x}^{(i)})$ and the average of $g^{\text{MGBM}}(\mathbf{X})$ associated with some input feature X_j [54]. Accordingly, the logit of the sum of the Shapley values and the Shapley intercept will be the $g^{\text{MGBM}}(\mathbf{x})$ prediction in the probability space, for any \mathbf{x} .

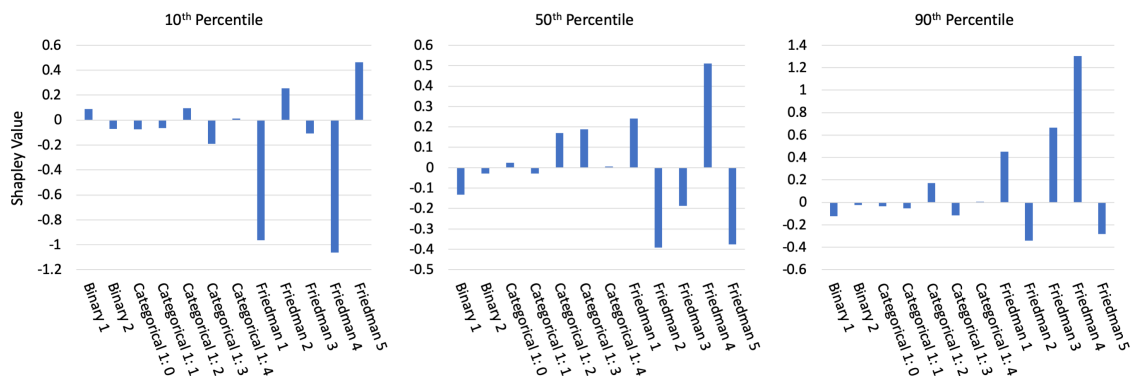


Figure A3. Tree SHAP values for three observations across selected percentiles of $g^{\text{MGBM}}(\mathbf{X})$ for the simulated test data.

The Shapley values in Figure A3 appear to be a logical result. For the lower prediction at the 10th percentile of $g^{\text{MGBM}}(\mathbf{X})$, the largest local contributions are negative and the majority of local contributions are also negative. At the median of $g^{\text{MGBM}}(\mathbf{X})$, local contributions are roughly split

between positive and negative values, and at the 90th of $g^{\text{MGBM}}(\mathbf{X})$, most large contributions are positive. In each case, large local contributions generally follow global importance results in Figure A1 as well.

Figure A4 shows global mean absolute Shapley feature importance for g^{XNN} on the simulated test data, using the approximate Deep SHAP technique. Deep SHAP values are reported in the probability space, after the application of the logit link function. They are also calculated from the projection layer of g^{XNN} . Thus, the Deep SHAP values in Figure A4 are the estimated average absolute impact of each X_j in the projection layer and probability space of g^{XNN} for the simulated test data.

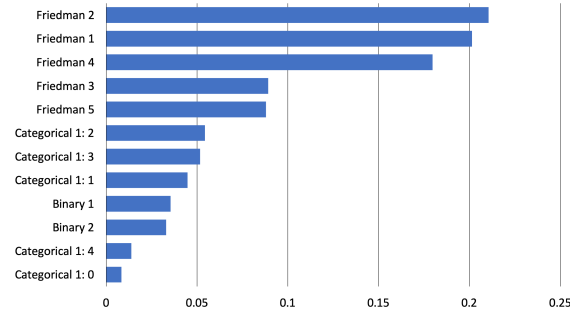


Figure A4. Global mean Deep SHAP feature importance for $g^{\text{XNN}}(\mathbf{X})$ on the simulated test data.

Like g^{MGBM} , g^{XNN} ranks the $X_{\text{Friedman},j}$ features higher in terms of importance than the categorical and binary features. The consistency between the feature rankings of g^{MGBM} and g^{XNN} is somewhat striking, given their different hypothesis families and architectures. Both g^{MGBM} and g^{XNN} rank $X_{\text{Friedman},1}$, $X_{\text{Friedman},2}$, and $X_{\text{Friedman},4}$ as the most important features, both place $X_{\text{Categorical},2}$ and $X_{\text{Categorical},3}$ above the $X_{\text{Binary},1}$ and $X_{\text{Binary},2}$ features, both rank $X_{\text{Binary},1}$ above $X_{\text{Binary},2}$, and both place the least importance on $X_{\text{Categorical},4}$ and $X_{\text{Categorical},0}$.

Figure A5 provides detailed insights into g^{XNN} . A5 A displays the sparse γ_k weights of the output layer, where only n_k subnetworks with $k \in \{1, 4, 7, 8, 9\}$ are associated with large magnitude weights. The n_k subnetwork ridge functions appear in A5 B as simplistic but distinctive functional forms. Color-coding between A5 A and A5 B visually reinforces the direct feed-forward relationship between the n_k subnetworks and the γ_k weights of the output layer.

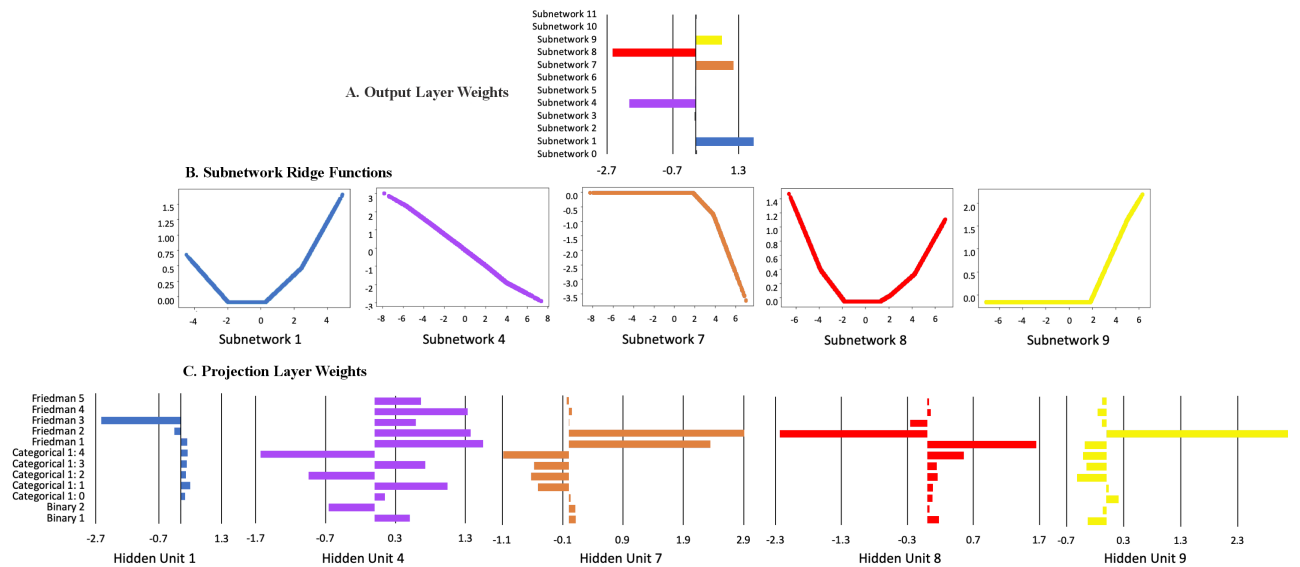


Figure A5. A. Output layer γ_k weights, B. corresponding n_k ridge functions, and C. associated projection layer β_j weights for g^{XNN} on the simulated test data.

n_k subnetworks are plotted across the output values of their associated $\sum_j \beta_{k,j} x_j$ projection layer hidden units, and color-coding between A5 B and A5 C link the β_j weights to their n_k subnetworks. Most of the heavily utilized n_k subnetworks have sparse weights in their $\sum_j \beta_{k,j} x_j$ projection layer hidden units. In particular, subnetwork n_1 appears to be almost solely a function of $X_{\text{Friedman},3}$ and appears to exhibit the expected quadratic behavior for $X_{\text{Friedman},3}$. Subnetworks n_7 , n_8 , and n_9 appear to be most associated with the globally important $X_{\text{Friedman},1}$ and $X_{\text{Friedman},2}$ features, likely betraying the effort required for g^{XNN} to model the nonlinear $\sin()$ function of the $X_{\text{Friedman},1}$ and $X_{\text{Friedman},2}$ product, and n_7 , n_8 , and n_9 do appear to display some noticeable sinusoidal characteristics. Conversely, subnetwork n_4 seems to be a linear combination of all the original input X_j features, but does weigh the linear $X_{\text{Friedman},4}$ and $X_{\text{Friedman},5}$ terms roughly in the correct two-to-one ratio. As a whole, Figure A5 A, B, and C exhibit evidence that $g^{\text{XNN}}(\mathbf{X})$ has learned about the simulated function in Equation 1 and the displayed information should help practitioners understand which original input X_j features are weighed heavily in each n_k subnetwork, and which n_k subnetworks have a strong influence on $g^{\text{XNN}}(\mathbf{X})$.

Local Deep SHAP feature importance in Figure A6 supplements the global interpretability of g^{XNN} displayed in Figures A4 and A5. Local Deep SHAP values are extracted from the projection layer of g^{XNN} and reported in the probability space. Deep SHAP values can be calculated for any arbitrary $g^{\text{XNN}}(\mathbf{x})$, allowing for detailed, local summarization of individual model predictions.

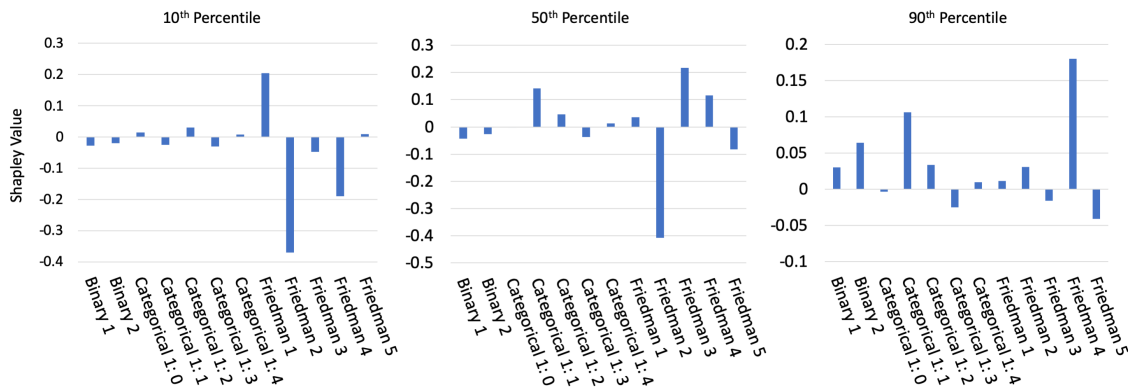


Figure A6. Deep SHAP values for three observations across selected percentiles of $g^{\text{XNN}}(\mathbf{X})$ on the simulated test data.

As expected, Deep SHAP values generally increase from the 10th percentile of $g^{\text{XNN}}(\mathbf{X})$ to the 90th percentile of $g^{\text{XNN}}(\mathbf{X})$, with primarily important global drivers of model behavior contributing to the selected local $g^{\text{XNN}}(\mathbf{x}^{(i)})$ predictions.

Appendix E.3. Discrimination Testing Results

Tables A2a and A2b show the results of the disparity tests using the simulated data for two hypothetical sets of class-control groups. Several measures of disparities are shown, with the SMDs calculated using the probabilities from g^{MGBM} and g^{XNN} , and the false positive rates (FPRs), false negative rates (FNRs), their ratios, MEs, and AIRs calculated using a binary outcome based on a cutoff of 0.6 (anyone with probabilities of 0.6 or greater receives the favorable outcome).²⁴

Since g^{MGBM} and g^{XNN} assume that a higher score is favorable (as might be the case if the model were predicting responses to marketing offers), one might consider the relative FNRs as a measure of the class-control disparities. Table A2b shows that protected group 1 has higher relative FNRs under g^{XNN} (1.13 vs. 1.06). However, in Table A2a the overall FNRs were lower for g^{XNN} (0.357 vs. 0.401).

²⁴ See Appendix F for comments pertaining to cutoff selection and discrimination testing.

This illustrates a danger in considering relative class-control metrics in isolation when comparing across models: despite the g^{MGBM} appearing to be a relatively fairer model, more protected group 1 members experience negative outcomes using g^{MGBM} . This is because FNR accuracy improves for both the protected group 1 and control group 1, but members of control group 1 benefit more than those in protected group 1. Of course, the choice of which model is truly fairer is a policy question.

(a) Group size, accuracy, and FNR for g^{MGBM} and g^{XNN} on the simulated test data.

Class	N	Model	Accuracy	FNR
Protected 1	3,057	g^{MGBM}	0.770	0.401
		g^{XNN}	0.771	0.357
Control 1	16,943	g^{MGBM}	0.739	0.378
		g^{XNN}	0.756	0.314
Protected 2	9,916	g^{MGBM}	0.758	0.331
		g^{XNN}	0.762	0.302
Control 2	10,084	g^{MGBM}	0.729	0.420
		g^{XNN}	0.756	0.332

(b) AIR, ME, SMD, and FNR ratio for g^{MGBM} and g^{XNN} on the simulated test data.

Model	Protected Class	Control Class	AIR	ME	SMD	FNR Ratio
g^{MGBM}	1	1	0.752	9.7%	-0.206	1.06
	2	2	1.10	-3.6%	0.106	0.788
g^{XNN}	1	1	0.727	12.0%	-0.274	1.13
	2	2	0.976	1.0%	0.001	0.907

Table A2. Discrimination measures for the simulated test data.

For g^{XNN} , 12.0% fewer control group 1 members receive the favorable offer under the ME column in Table A2b. Of note is that 12.0% is not a meaningful difference without context. If the population of control group 1 and control group 2 were substantially similar in relevant characteristics, 12.0% could represent an extremely large difference and would require remediation. But if they represent substantially different populations, then 12.0% could represent a reasonable deviation from parity. As an example, if a lending institution that has traditionally focused on high credit quality clients were to expand into previously under-banked communities, a 12.0% class-control difference in loan approval rates might be expected because the average credit quality of the new population would be lower than that of the existing population. Protected group 1's AIR under g^{XNN} is 0.727, below the EEOC 4/5ths rule threshold. It is also highly statistically significant (not shown, but available in resources discussed in Subsection 1.8). Together these would indicate that there may be evidence of illegal DI. As with ME and other measures, the reasonableness of this disparity is not clear outside of context. However, most regulated institutions that do perform discrimination analyses would find an AIR of this magnitude concerning and warranting further review. Some pertinent remediation strategies for discovered discrimination are discussed in Section 3.3.

SMD is used here to measure $g^{MGBM}(X)$ and $g^{XNN}(X)$ probabilities prior to being transformed into classifications. (This measurement would be particularly relevant if the probabilities are used in combination with other models to determine an outcome.) The results show that g^{MGBM} has less disparate impact than g^{XNN} (-0.206 vs. -0.274), but both are close to Cohen's small effect threshold of -0.20. Whether a small effect would be a highlighted concern would depend on an organization's chosen threshold for flagging models for further review.

Appendix F. Cutoff Selection w.r.t Mitigating Discrimination

The selection of which cutoff to use in production is typically based on the model's use case, rather than one based solely on the statistical properties of the predictions themselves. For example, a model developer at a bank might build a credit model where the F1 score is maximized at a delinquency probability cutoff of 0.15. For purposes of evaluating the quality of the model, she may review confusion matrix statistics (accuracy, recall, precision, etc.) using cutoffs based on the maximum F1 score. But, because of its risk tolerance and other factors, the bank itself might be willing to lend to anyone with a delinquency probability of 0.18 or lower, which would mean that anyone who is scored

at 0.18 or lower would receive an offer of credit. Because disparity analyses are concerned with how people are affected by the way the model is used, it is essential that any confusion matrix-based metrics of disparity be calculated on the in-production classification decisions, rather than the cutoffs that are not related to what those affected by the model will experience.

Appendix G. Recent Fairness Techniques and Compliance

Great care must be taken in order to ensure that the appropriate fairness metrics are chosen, because certain metrics may not be appropriate for some use cases. Additionally, the effects of changing the model must be viewed holistically. For example, the mortgage data disparity analysis in Section 2.1.3 shows that if one were to choose g^{MGBM} over g^{XNN} because g^{MGBM} has a lower FPR ratio for blacks, it would ultimately lead to a higher FPR for blacks overall, which may represent doing more harm than good.

Furthermore, using some recently developed discrimination mitigation methods may lead to non-compliance with anti-discrimination laws and regulations. A fundamental maxim of US anti-discrimination law is that (to slightly paraphrase), “similarly situated people should be treated similarly.”²⁵ A model developed without inclusion of class status (or proxies thereof) considers similarly situated people the same on the dimensions included in the model: people who have the same feature values will have the same model output (though there may be some small or random differences in outcomes due to computational issues). Obviously, the inclusion of protected class status will change model output by class. With possible rare exceptions, this is likely to be viewed with legal and regulatory skepticism today, even if including class status is done with fairness as the goal.²⁶ Preprocessing and post-processing techniques may be similarly problematic, because industries that must provide explanations to those who receive unfavorable treatment (e.g., adverse action notices in US financial services) may have to incorporate the class adjustments into their explanations as well.

References

1. Rudin, C. Please Stop Explaining Black Box Models for High Stakes Decisions and Use Interpretable Models Instead. *arXiv preprint arXiv:1811.10154* 2018. URL: <https://arxiv.org/pdf/1811.10154.pdf>.
2. Feldman, M.; Friedler, S.A.; Moeller, J.; Scheidegger, C.; Venkatasubramanian, S. Certifying and Removing Disparate Impact. *Proceedings of the 21st ACM SIGKDD International Conference on Knowledge Discovery and Data Mining*. ACM, 2015, pp. 259–268. URL: <https://arxiv.org/pdf/1412.3756.pdf>.
3. Dwork, C.; Hardt, M.; Pitassi, T.; Reingold, O.; Zemel, R. Fairness Through Awareness. *Proceedings of the 3rd Innovations in Theoretical Computer Science Conference*. ACM, 2012, pp. 214–226. URL: <https://arxiv.org/pdf/1104.3913.pdf>.
4. Buolamwini, J.; Gebru, T. Gender Shades: Intersectional Accuracy Disparities in Commercial Gender Classification. *Conference on Fairness, Accountability and Transparency*, 2018, pp. 77–91. URL: <http://proceedings.mlr.press/v81/buolamwini18a/buolamwini18a.pdf>.
5. Barreno, M.; Nelson, B.; Joseph, A.D.; Tygar, J. The Security of Machine Learning. *Machine Learning* 2010, 81, 121–148. URL: http://people.ischool.berkeley.edu/~tygar/papers/SML/sec_mach_learn_journal.pdf.
6. Tramèr, F.; Zhang, F.; Juels, A.; Reiter, M.K.; Ristenpart, T. Stealing Machine Learning Models via Prediction APIs. 25th {USENIX} Security Symposium ({USENIX} Security 16), 2016, pp. 601–618. URL: https://www.usenix.org/system/files/conference/usenixsecurity16/sec16_paper_tramer.pdf.

²⁵ In the pay discrimination case, *Bazemore v. Friday*, 478 US 385 (1986), the US Supreme Court found that, “Each week’s paycheck that delivers less to a black than to a similarly situated white is a wrong actionable ...” Beyond the obvious conceptual meaning, what specifically constitutes *similarly situated* is controversial and its interpretation differs by circuit.

²⁶ In a reverse discrimination case, *Ricci v. Desafano*, 557 US 557 (2009), the court found that any consideration of race which is not justified by correcting for past proven discrimination is illegal and, moreover, a lack of fairness is not necessarily evidence of illegal discrimination.

7. Shokri, R.; Stronati, M.; Song, C.; Shmatikov, V. Membership Inference Attacks Against Machine Learning Models. 2017 IEEE Symposium on Security and Privacy (SP). IEEE, 2017, pp. 3–18. URL: <https://arxiv.org/pdf/1610.05820.pdf>.
8. Shokri, R.; Strobel, M.; Zick, Y. Privacy Risks of Explaining Machine Learning Models. *arXiv preprint arXiv:1907.00164* 2019. URL: <https://arxiv.org/pdf/1907.00164.pdf>.
9. Williams, M.; others. *Interpretability*; Fast Forward Labs, 2017. URL: <https://www.cloudera.com/products/fast-forward-labs-research.html>.
10. Friedman, J.H. A Tree-structured Approach to Nonparametric Multiple Regression. In *Smoothing techniques for curve estimation*; Springer, 1979; pp. 5–22. URL: <http://inspirehep.net/record/140963/files/slac-pub-2336.pdf>.
11. Friedman, J.H.; others. Multivariate Adaptive Regression Splines. *The annals of statistics* **1991**, 19, 1–67. URL: https://projecteuclid.org/download/pdf_1/euclid.aos/1176347963.
12. Friedman, J.H. Greedy Function Approximation: a Gradient Boosting Machine. *Annals of statistics* **2001**, pp. 1189–1232. URL: https://projecteuclid.org/download/pdf_1/euclid.aos/1013203451.
13. Friedman, J.H.; Hastie, T.; Tibshirani, R. *The Elements of Statistical Learning*; Springer: New York, 2001. URL: https://web.stanford.edu/~hastie/ElemStatLearn/printings/ESLII_print12.pdf.
14. Recht, B.; Re, C.; Wright, S.; Niu, F. HOGWILD: A Lock-free Approach to Parallelizing Stochastic Gradient Descent. *Advances in Neural Information Processing Systems (NIPS)*, 2011, pp. 693–701. URL: <https://papers.nips.cc/paper/4390-hogwild-a-lock-free-approach-to-parallelizing-stochastic-gradient-descent.pdf>.
15. Hinton, G.E.; Srivastava, N.; Krizhevsky, A.; Sutskever, I.; Salakhutdinov, R.R. Improving Neural Networks by Preventing Co-adaptation of Feature Detectors. *arXiv preprint arXiv:1207.0580* 2012. URL: <https://arxiv.org/pdf/1207.0580.pdf>.
16. Sutskever, I.; Martens, J.; Dahl, G.; Hinton, G. On the Importance of Initialization and Momentum in Deep Learning. *International Conference on Machine Learning*, 2013, pp. 1139–1147. URL: <http://proceedings.mlr.press/v28/sutskever13.pdf>.
17. Zeiler, M.D. ADADELTA: an Adaptive Learning Rate Method. *arXiv preprint arXiv:1212.5701* 2012. URL: <https://arxiv.org/pdf/1212.5701.pdf>.
18. Aivodji, U.; Arai, H.; Fortineau, O.; Gambs, S.; Hara, S.; Tapp, A. Fairwashing: the Risk of Rationalization. *arXiv preprint arXiv:1901.09749* 2019. URL: <https://arxiv.org/pdf/1901.09749.pdf>.
19. Slack, D.; Hilgard, S.; Jia, E.; Singh, S.; Lakkaraju, H. How Can We Fool LIME and SHAP? Adversarial Attacks on Post-hoc Explanation Methods. *arXiv preprint arXiv:1911.02508* 2019. URL: <https://arxiv.org/pdf/1911.02508.pdf>.
20. Vaughan, J.; Sudjianto, A.; Brahimi, E.; Chen, J.; Nair, V.N. Explainable Neural Networks Based on Additive Index Models. *arXiv preprint arXiv:1806.01933* 2018. URL: <https://arxiv.org/pdf/1806.01933.pdf>.
21. Yang, Z.; Zhang, A.; Sudjianto, A. Enhancing Explainability of Neural Networks Through Architecture Constraints. *arXiv preprint arXiv:1901.03838* 2019. URL: <https://arxiv.org/pdf/1901.03838.pdf>.
22. Goldstein, A.; Kapelner, A.; Bleich, J.; Pitkin, E. Peeking Inside the Black Box: Visualizing Statistical Learning with Plots of Individual Conditional Expectation. *Journal of Computational and Graphical Statistics* **2015**, 24. URL: <https://arxiv.org/pdf/1309.6392.pdf>.
23. Lundberg, S.M.; Lee, S.I. A Unified Approach to Interpreting Model Predictions. In *Advances in Neural Information Processing Systems (NIPS)*; Guyon, I.; Luxburg, U.V.; Bengio, S.; Wallach, H.; Fergus, R.; Vishwanathan, S.; Garnett, R., Eds.; Curran Associates, Inc., 2017; pp. 4765–4774. URL: <http://papers.nips.cc/paper/7062-a-unified-approach-to-interpreting-model-predictions.pdf>.
24. Lundberg, S.M.; Erion, G.G.; Lee, S.I. Consistent Individualized Feature Attribution for Tree Ensembles. In *Proceedings of the 2017 ICML Workshop on Human Interpretability in Machine Learning (WHI 2017)*; Kim, B.; Malioutov, D.M.; Varshney, K.R.; Weller, A., Eds.; ICML WHI 2017, 2017; pp. 15–21. URL: <https://openreview.net/pdf?id=ByTKSo-m->.
25. Cohen, J. *Statistical Power Analysis for the Behavioral Sciences*; Lawrence Erlbaum Associates, 1988. URL: <http://www.utstat.toronto.edu/~brunner/oldclass/378f16/readings/CohenPower.pdf>.
26. Cohen, J. A Power Primer. *Psychological Bulletin* **1992**, 112, 155. URL: <https://www.ime.usp.br/~abe/lista/pdfn45sGokvRe.pdf>.

27. Zafar, M.B.; Valera, I.; Gomez Rodriguez, M.; Gummadi, K.P. Fairness Beyond Disparate Treatment & Disparate Impact: Learning Classification Without Disparate Mistreatment. *Proceedings of the 26th International Conference on World Wide Web. International World Wide Web Conferences Steering Committee*, 2017, pp. 1171–1180. URL: <https://arxiv.org/pdf/1610.08452.pdf>.
28. Lou, Y.; Caruana, R.; Gehrke, J.; Hooker, G. Accurate Intelligible Models with Pairwise Interactions. *Proceedings of the 19th ACM SIGKDD International Conference on Knowledge Discovery and Data Mining. ACM*, 2013, pp. 623–631. URL: <http://citeseerx.ist.psu.edu/viewdoc/download?doi=10.1.1.352.7682&rep=rep1&type=pdf>.
29. Apley, D.W. Visualizing the Effects of Predictor Variables in Black Box Supervised Learning Models. *arXiv preprint arXiv:1612.08468* **2016**. URL: <https://arxiv.org/pdf/1612.08468.pdf>.
30. Shapley, L.S.; Roth, A.E.; others. *The Shapley value: Essays in Honor of Lloyd S. Shapley*; Cambridge University Press, 1988. URL: <http://www.library.fu.ru/files/Roth2.pdf>.
31. Hall, P. On the Art and Science of Machine Learning Explanations. *KDD '19 XAI Workshop Proceedings*, 2019. URL: <https://arxiv.org/pdf/1810.02909.pdf>.
32. Hu, X.; Rudin, C.; Seltzer, M. Optimal Sparse Decision Trees. *arXiv preprint arXiv:1904.12847* **2019**. URL: <https://arxiv.org/pdf/1904.12847.pdf>.
33. Friedman, J.H.; Popescu, B.E.; others. Predictive Learning Via Rule Ensembles. *The Annals of Applied Statistics* **2008**, 2, 916–954. URL: https://projecteuclid.org/download/pdfview_1/euclid.aoas/1223908046.
34. Gupta, M.; Cotter, A.; Pfeifer, J.; Voevodski, K.; Canini, K.; Mangylov, A.; Moczydlowski, W.; Van Esbroeck, A. Monotonic Calibrated Interpolated Lookup Tables. *The Journal of Machine Learning Research* **2016**, 17, 3790–3836. URL: <http://www.jmlr.org/papers/volume17/15-243/15-243.pdf>.
35. Chen, C.; Li, O.; Barnett, A.; Su, J.; Rudin, C. This Looks Like That: Deep Learning for Interpretable Image Recognition. *Proceedings of Neural Information Processing Systems (NeurIPS)*, 2019. URL: <https://arxiv.org/pdf/1806.10574.pdf>.
36. Wilkinson, L. Visualizing Big Data Outliers through Distributed Aggregation. *IEEE Transactions on Visualization & Computer Graphics* **2018**. URL: <https://www.cs.uic.edu/~wilkinson/Publications/outliers.pdf>.
37. Udell, M.; Horn, C.; Zadeh, R.; Boyd, S.; others. Generalized Low Rank Models. *Foundations and Trends® in Machine Learning* **2016**, 9, 1–118. URL: <https://www.nowpublishers.com/article/Details/MAL-055>.
38. Holohan, N.; Braghin, S.; Mac Aonghusa, P.; Levacher, K. Diffprivlib: The IBM Differential Privacy Library. *arXiv preprint arXiv:1907.02444* **2019**. URL: <https://arxiv.org/pdf/1907.02444.pdf>.
39. Ji, Z.; Lipton, Z.C.; Elkan, C. Differential Privacy and Machine Learning: A Survey and Review. *arXiv preprint arXiv:1412.7584* **2014**. URL: <https://arxiv.org/pdf/1412.7584.pdf>.
40. Papernot, N.; Song, S.; Mironov, I.; Raghunathan, A.; Talwar, K.; Erlingsson, Ú. Scalable Private Learning with PATE. *arXiv preprint arXiv:1802.08908* **2018**. URL: <https://arxiv.org/pdf/1802.08908.pdf>.
41. Abadi, M.; Chu, A.; Goodfellow, I.; McMahan, H.B.; Mironov, I.; Talwar, K.; Zhang, L. Deep Learning with Differential Privacy. *Proceedings of the 2016 ACM SIGSAC Conference on Computer and Communications Security. ACM*, 2016, pp. 308–318. URL: <https://arxiv.org/pdf/1607.00133.pdf>.
42. Wachter, S.; Mittelstadt, B.; Russell, C. Counterfactual Explanations without Opening the Black Box: Automated Decisions and the GDPR. *Harv. JL & Tech.* **2017**, 31, 841. URL: <https://arxiv.org/pdf/1711.00399.pdf>.
43. Ancona, M.; Ceolini, E.; Oztireli, C.; Gross, M. Towards Better Understanding of Gradient-based Attribution Methods for Deep Neural Networks. *6th International Conference on Learning Representations (ICLR 2018)*, 2018. URL: https://www.research-collection.ethz.ch/bitstream/handle/20.500.11850/249929/Flow_ICLR_2018.pdf.
44. Wallace, E.; Tuyls, J.; Wang, J.; Subramanian, S.; Gardner, M.; Singh, S. AllenNLP Interpret: A Framework for Explaining Predictions of NLP Models. *arXiv preprint arXiv:1909.09251* **2019**. URL: <https://arxiv.org/pdf/1909.09251.pdf>.
45. Kamiran, F.; Calders, T. Data Preprocessing Techniques for Classification Without Discrimination. *Knowledge and Information Systems* **2012**, 33, 1–33. URL: <https://bit.ly/2IH95lQ>.
46. Zhang, B.H.; Lemoine, B.; Mitchell, M. Mitigating Unwanted Biases with Adversarial Learning. *Proceedings of the 2018 AAAI/ACM Conference on AI, Ethics, and Society. ACM*, 2018, pp. 335–340. URL: <https://arxiv.org/pdf/1801.07593.pdf>.

47. Zemel, R.; Wu, Y.; Swersky, K.; Pitassi, T.; Dwork, C. Learning Fair Representations. International Conference on Machine Learning, 2013, pp. 325–333. URL: <http://proceedings.mlr.press/v28/zemel13.pdf>.
48. Kamiran, F.; Karim, A.; Zhang, X. Decision Theory for Discrimination-aware Classification. 2012 IEEE 12th International Conference on Data Mining. IEEE, 2012, pp. 924–929. URL: <http://citeseerx.ist.psu.edu/viewdoc/download?doi=10.1.1.722.3030&rep=rep1&type=pdf>.
49. Rauber, J.; Brendel, W.; Bethge, M. Foolbox: A Python Toolbox to Benchmark the Robustness of Machine Learning Models. *arXiv preprint arXiv:1707.04131* 2017. URL: <https://arxiv.org/pdf/1707.04131.pdf>.
50. Papernot, N.; Faghri, F.; Carlini, N.; Goodfellow, I.; Feinman, R.; Kurakin, A.; Xie, C.; Sharma, Y.; Brown, T.; Roy, A.; Matyasko, A.; Behzadan, V.; Hambardzumyan, K.; Zhang, Z.; Juang, Y.L.; Li, Z.; Sheatsley, R.; Garg, A.; Uesato, J.; Gierke, W.; Dong, Y.; Berthelot, D.; Hendricks, P.; Rauber, J.; Long, R. Technical Report on the CleverHans v2.1.0 Adversarial Examples Library. *arXiv preprint arXiv:1610.00768* 2018. URL: <https://arxiv.org/pdf/1610.00768.pdf>.
51. Amershi, S.; Chickering, M.; Drucker, S.M.; Lee, B.; Simard, P.; Suh, J. Modeltracker: Redesigning Performance Analysis Tools for Machine Learning. Proceedings of the 33rd Annual ACM Conference on Human Factors in Computing Systems. ACM, 2015, pp. 337–346. URL: <https://www.microsoft.com/en-us/research/wp-content/uploads/2016/02/amershi.CHI2015.ModelTracker.pdf>.
52. Papernot, N. A Marauder’s Map of Security and Privacy in Machine Learning: An overview of current and future research directions for making machine learning secure and private. Proceedings of the 11th ACM Workshop on Artificial Intelligence and Security. ACM, 2018. URL: <https://arxiv.org/pdf/1811.01134.pdf>.
53. Mitchell, M.; Wu, S.; Zaldivar, A.; Barnes, P.; Vasserman, L.; Hutchinson, B.; Spitzer, E.; Raji, I.D.; Gebru, T. Model Cards for Model Reporting. Proceedings of the Conference on Fairness, Accountability, and Transparency. ACM, 2019, pp. 220–229. URL: <https://arxiv.org/pdf/1810.03993.pdf>.
54. Molnar, C. *Interpretable Machine Learning*; christophm.github.io, 2018. URL: <https://christophm.github.io/interpretable-ml-book/>.
55. Bracke, P.; Datta, A.; Jung, C.; Sen, S. Machine Learning Explainability in Finance: an Application to Default Risk Analysis 2019. URL: <https://www.bankofengland.co.uk/-/media/boe/files/working-paper/2019/machine-learning-explainability-in-finance-an-application-to-default-risk-analysis.pdf>.
56. Friedler, S.A.; Scheidegger, C.; Venkatasubramanian, S.; Choudhary, S.; Hamilton, E.P.; Roth, D. A Comparative Study of Fairness-enhancing Interventions in Machine Learning. Proceedings of the Conference on Fairness, Accountability, and Transparency. ACM, 2019, pp. 329–338. URL: <https://arxiv.org/pdf/1802.04422.pdf>.
57. Schmidt, N.; Stephens, B. An Introduction to Artificial Intelligence and Solutions to the Problems of Algorithmic Discrimination. *arXiv preprint arXiv:1911.05755* 2019. URL: <https://arxiv.org/pdf/1911.05755.pdf>.
58. Hoare, C.A.R. The 1980 ACM Turing Award Lecture. *Communications* 1981. URL: <http://www.cs.fsu.edu/~engelen/courses/COP4610/hoare.pdf>.